A Novel Approach to Identify the Effect of Correlated Colour Temperatures on Behavioural and Neurocognitive Performance in a Virtual Reality Based Simulated Platform and Validation of the same

Thesis submitted in partial fulfilment of the requirements for award of the degree of Master of Engineering in Illumination Engineering

Submitted by

SREEMANTI BASU

Exam Roll No: M4ILN24006

Class Roll No: 002210805006

Registration No: 163499 of 2022-2023

Session: 2022-2023

Under the supervision of

Dr. SUDDHASATWA CHAKRABORTY

Associate Professor
Electrical Engineering Department
Jadavpur University

Department of Electrical Engineering

Jadavpur University,

Kolkata-700032.

August, 2024

Jadavpur University
Faculty of Engineering and Technology
Department of Electrical Engineering

CERTIFICATE OF RECOMMENDATION

This is to certify that the thesis entitled **"A Novel Approach to Identify the Effect of Correlated Colour Temperatures on Behavioural and Neurocognitive Performance in a Virtual Reality Based Simulated Platform and Validation of the same"** submitted by **SREEMANTI BASU**, (Examination Roll No. **M4ILN24006**, Registration No. **163499 of 2022-2023**) of this University in partial fulfilment of requirements for the award of the degree of Master of Engineering in Illumination Engineering, Department of Electrical Engineering, is a bonafide record of the work carried out by her under my guidance and supervision.

(Thesis supervisor)
Dr. SUDDHASATWA CHAKRABORTY
Associate Professor
Electrical Engineering Department
Jadavpur University
Kolkata- 700032

Prof. (Dr.) BISWANATH ROY
Head of the Department
Electrical Engineering Department
Jadavpur University
Kolkata- 700032

Prof. (Dr.) DIPAK LAHA
Dean
Faculty of Engineering and Technology
Jadavpur University
Kolkata- 700032

Jadavpur University
Faculty of Engineering and Technology
Department of Electrical Engineering

CERTIFICATE OF APPROVAL

This foregoing thesis is hereby approved as a creditable study in the area of Illumination Engineering, carried out and presented by **SREEMANTI BASU**, in a manner of satisfactory, warrant its acceptance as a pre-requisite to the degree for which it has been submitted. It is notified to understood that by this approval, the undersigned does not necessarily endorse or approved the thesis only for the purpose for which it has been submitted.

FINAL EXAMINATION FOR EVALUATION OF THESIS

BOARD OF EXAMINERS

…….

…….

…….

(Signature of Examiners)

Jadavpur University

Declaration of Originality and Compliance of Academic Ethics

I hereby declare that this thesis contains a literature survey and original research work by the undersigned candidate, as part of my Master of Engineering in Illumination Engineering studies.

All information in this document has been obtained and presented in accordance with academic rules and ethical conduct.

I also declare that, as required by these rules and conduct, I have fully cited and referred all material and results that are not original to this work.

Name	**:**	**SREEMANTI BASU**
Examination Roll No.	**:**	**M4ILN24006**
Registration No.	**:**	**163499 of 2022-2023**
Thesis Title	**:**	**A Novel Approach to Identify the Effect of Correlated Colour Temperatures on Behavioural and Neurocognitive Performance in a Virtual Reality Based Simulated Platform and Validation of the same**
Signature	**:**	
Date	**:**	

ACKNOWLEDGEMENT

I would like to take this opportunity to express my deepest gratitude and appreciation to Dr. Suddhasatwa Chakraborty, Associate Professor, Department of Electrical Engineering at Jadavpur University, Kolkata, without whose insightful vision and guidance, this project could not have been accomplished.

I also wish to extend my heartfelt thanks to Prof. (Dr.) Biswanath Roy, Head of the Department of Electrical Engineering at Jadavpur University, Kolkata, for his valuable academic guidance and for granting me the opportunity to conduct my project work in the Illumination Engineering Laboratory at Jadavpur University.

Additionally, I am sincerely grateful to Prof. (Dr.) Saswati Mazumdar, Professor in the Department of Electrical Engineering at Jadavpur University, Kolkata, and Sangita Sahana, Assistant Professor in the same department, for their continuous academic support and guidance throughout this project.

I am also thankful to all laboratory assistants of the Illumination Engineering Laboratory for their co-operation during my project work.

I want convey my thanks to my classmates Roni Jana, Biswanil Khan, Prasanjit Ghosh, Triparna Mondal and Avijit Bid for their steadfast assistance.

Last but not the least, I wish to convey my sincere gratitude and thanks to my parents and brother for their unwavering support.

Place: Jadavpur University
Kolkata-700032

Date: SREEMANTI BASU

ABSTRACT

This study introduces a novel approach to exploring the impact of Correlated Colour Temperatures (CCTs) on behavioural and neurocognitive performance, within the context of human-centric lighting design. Utilizing a virtual reality (VR) simulation platform, the research examines how different CCTs influence cognitive functions, visual acuity, and task performance. The VR findings are validated through the usage of Landolt's Ring experiment, which measure visual acuity, and driving simulation tasks that assess object identification under varying lighting conditions. By integrating electroencephalogram (EEG) and galvanic skin response (GSR) measurements, the study provides a comprehensive analysis of both cognitive and physiological responses to different lighting environments. This research contributes to the development of human-centric lighting systems that optimize both mental and physical performance, particularly in environments demanding high levels of visual and cognitive precision.

Keywords: Correlated colour temperature (CCT), virtual reality (VR), visual acuity, peripheral vision, electroencephalogram (EEG), galvanic skin response (GSR)

CONTENTS

LIST OF FIGURES

LIST OF TABLES

CHAPTER 1

1.1 Introduction:

Virtual reality has become a highly effective and important tool in the field of vision science research. It plays a crucial role in advancing our understanding of visual processes by providing immersive and controlled environments for experimentation and study.

In VR, the CCT of virtual lighting can significantly influence the realism and comfort of the experience. Higher CCTs can enhance visual clarity and contrast, which is particularly important for tasks requiring precision and detailed observation. Adjusting CCT in VR can also affect the user's emotional response and immersion. Warmer light can create a more relaxing and comfortable atmosphere, while cooler light can increase alertness and focus.

Visual acuity in VR is the ability to see fine details within the virtual environment. High visual acuity is crucial for tasks that require detail recognition, such as reading text or identifying small objects. In VR, higher CCT lighting can enhance visual acuity by increasing contrast and making fine details more discernible. This is particularly important in VR applications that simulate work environments or tasks that require precision.

Peripheral vision in VR is essential for creating a sense of presence and realism. It allows users to detect movement and changes in the environment outside their direct line of sight, contributing to situational awareness. While peripheral vision is less sensitive to fine details, appropriate CCT can improve overall visibility and contrast in the periphery, making it easier to detect objects and movement. This can enhance the immersive experience by providing more realistic and responsive environments.

Object identification in VR involves recognizing and interacting with objects within the virtual space. Accurate object identification is essential for tasks such as gaming, training simulations, and virtual design. The CCT of virtual lighting

can impact how easily objects are identified. Higher CCTs can improve the identification of objects by enhancing contrast and detail, which is crucial for tasks that require quick and accurate recognition. The choice of CCT in VR affects visual acuity, peripheral vision, and object identification, all of which are critical for creating a realistic and functional virtual environment. Higher CCT can improve clarity and detail, aiding in tasks that require precision, while appropriate lighting can enhance peripheral vision and object identification, contributing to a more immersive and interactive experience. The right balance of CCT can also affect user comfort and immersion. Warmer light may be more suitable for relaxed, exploratory VR experiences, while cooler light might be better for task-oriented applications that require focus and detail.

CCT, visual acuity, peripheral vision, and object identification are all interconnected within a VR environment. Properly tuning CCT can enhance visual performance, realism, and user comfort, making it a critical factor in the design and effectiveness of VR experiences.

Studying neurocognitive and behavioural performance in both virtual reality (VR) and real-world environments provides valuable insights into how cognitive functions and behaviours vary across different contexts. VR offers a controlled setting that enables researchers to isolate and examine specific variables and conditions in detail. Nevertheless, validating these findings in real-world scenarios is crucial to ensure they accurately reflect actual behaviours and situations. The impact of lighting and correlated colour temperature (CCT) on neurocognitive and behavioural performance is significant for both VR simulations and real-world applications. In both environments, optimal lighting can improve performance by alleviating visual discomfort and enhancing cognitive function. While VR allows for precise investigation of these effects, real-world studies provide practical applications and validation.

CHAPTER 2

2.1 Background of the work:

Humans possess a wide range of visual and non-visual responses to light where some immediate responses are pupil dilation, glare perception, mood etc. Human-centric lighting has been integrated and embedded with the thought of light and lighting as the mediators of visual, biological, and behavioural responses in human and, also encompassing traditional elements of lighting quality, those that are rooted in vision while acknowledging new insights about non visual responses to light.

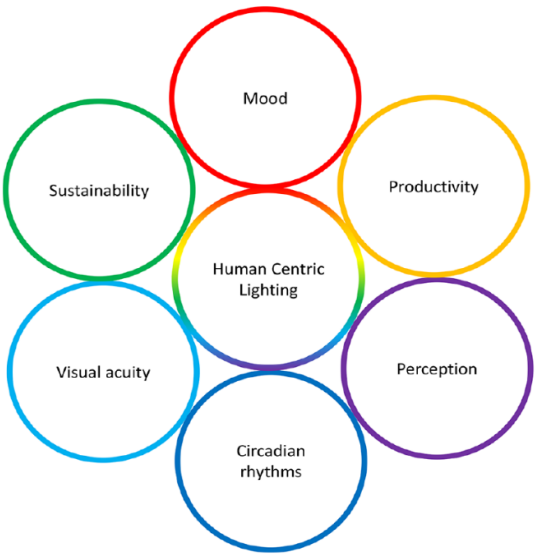

Figure 1 Human Centric lighting

Research into human behaviour in built environments is based on the notion that environments have a continuous influence on people. Hence human behaviour and preferences could be studied with the help of immersive technology like virtual environments that represents realism. These virtual environments allow the researchers and practitioners to manipulate their control variables while keeping other design features constant, resulting in more accurate experimental settings, and reduced experimental noise.

Virtual Reality (VR) is a technology that permits immersion of the user within the digital content, making them part of the simulated scenario, and replacing the physical world through different devices, basically it is an end-to-end mechanism. VR is used in many fields, from industrial design, robotics, gaming, to healthcare facilities. Since this technology has an ability to immerse participants in the virtual environment and isolate them from the outside world, it has great potential for conducting lighting research studies.

2.2 Virtual Reality:

Virtual Reality (VR) is a form of computer-implemented technology that allows a user to interact with a 3D artificial visual or sensory environment. The term virtual reality was coined in 1987 by Jaron Lanier, whose research and engineering contributed several products to the nascent VR industry. The 1950s and 1960s saw the emergence of virtual reality in several computing domains, most notably 3-D interactive computer graphics and vehicle/flight simulation.

In 1968 Ivan Sutherland at the University of Utah, with the help of his student Bob Sproull, created the first Virtual Reality (VR) and Augmented Reality (AR) head mounted display system. Sutherland's head mounted display was so heavy that it had to be suspended from the ceiling, and the formidable appearance of the device inspired its name—the Sword of Damocles. The system was rudimentary in terms of user interface and realism, with the graphics appearing as simple frame rooms for a Virtual Environment.

On the other hand, augmented reality highlighted the potential for immersive, real-time control systems for training and research as well as for enhanced performance. The idea behind augmented reality is to create a situation in which the user's environment is enhanced by virtual components.

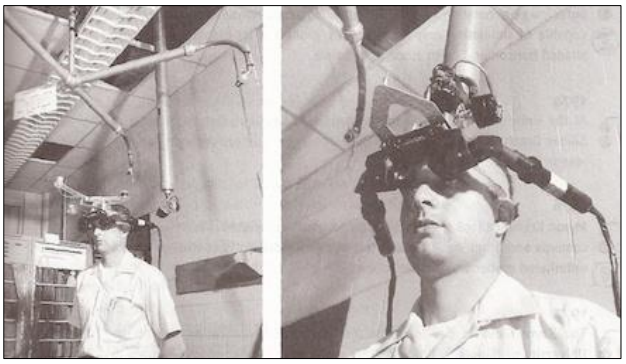

Figure 2

The first Virtual Reality (VR) and Augmented Reality (AR)

Figure 3

AR/VR model Meta Quest 3

2.3 Human Centric Lighting:

The essence of human-centric lighting is integrated thinking about light and lighting as mediators of visual, biological, and behavioural responses in humans. The phrase encompasses much because humans have such a wide range of visual and non-visual responses to light. Human-centric lighting is lighting designed to deliver a specified set of visual, biological, and behavioural responses identified as appropriate for the users of that lighting. Indeed, this is what good lighting has always been. But, with growing knowledge about the role of light and lighting on non-visual responses, the lighting community is faced with an expanding set of considerations and responsibilities [KW Houser et al]

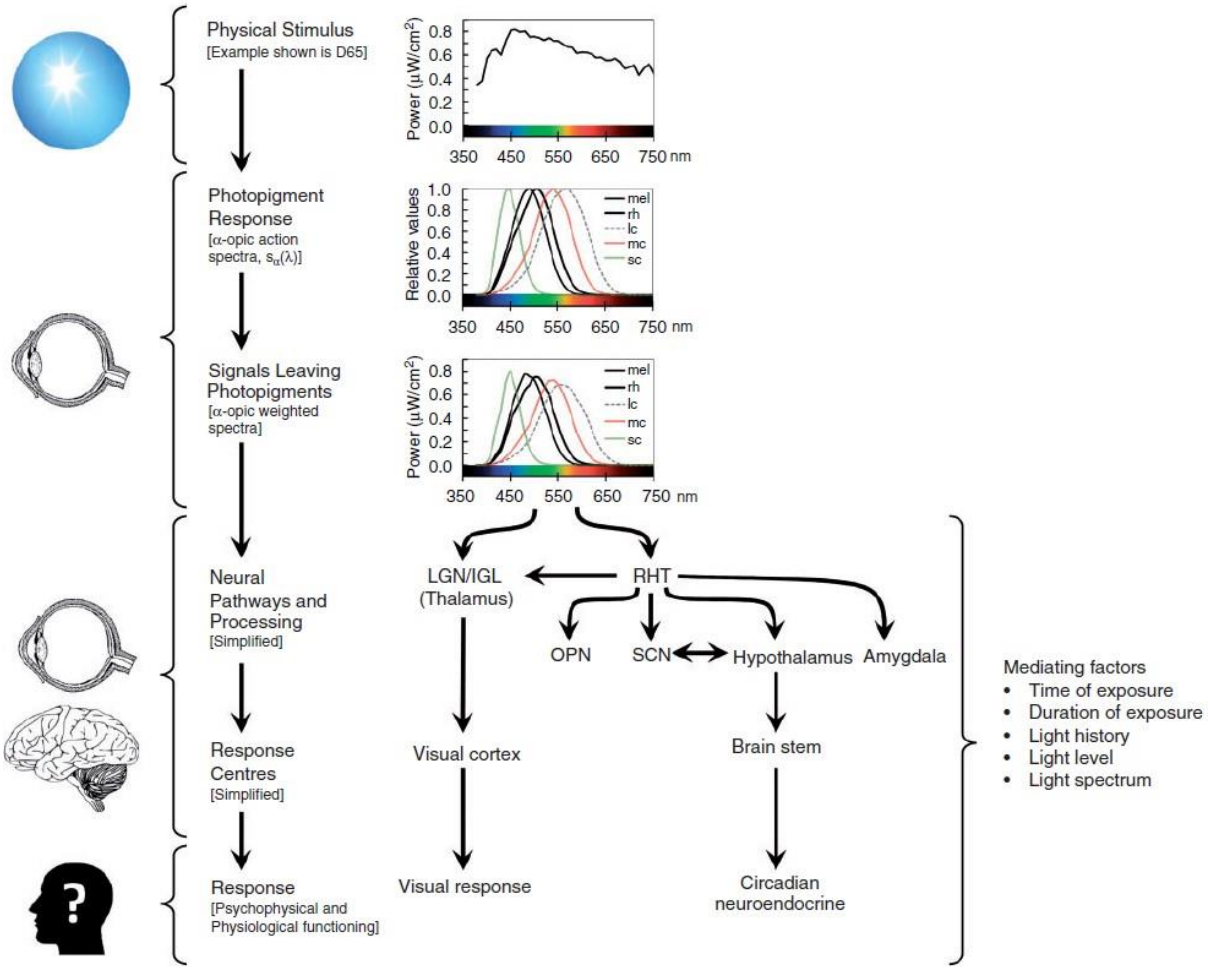

Figure 4 This schematic begins with light as a physical stimulus, which is transduced through the neuroanatomical underpinnings of eye–brain physiology, culminating with visual and non-visual responses. Cones and rods transmit light information via the lateral geniculate nucleus (LGN) and intergeniculate leaflet (IGL), continuing to the visual cortex. The melanopsin-containing ipRGCs generate and intrinsic melanopsin-driven response and receive extrinsic input from some rods and cones; the signal leaving the ipRGCs is a function of both their intrinsic response and extrinsic input. The ipRGCs transmit light information via the retino-hypothalamic tract (RHT) to the suprachiasmatic nuclei (SCN), which is the central clock in the brain. Other direct projections of the ipRGCs include the olivary pretectal nucleus (OPN, pupil constriction), hypothalamic nuclei (including the ventrolateral preoptic nucleus, involved in sleep regulation) and amygdala (involved in emotion regulation). The specific ipRGC-influenced light response will depend on the mediating factors shown to the right. Complexity and uncertainty increase from top to bottom

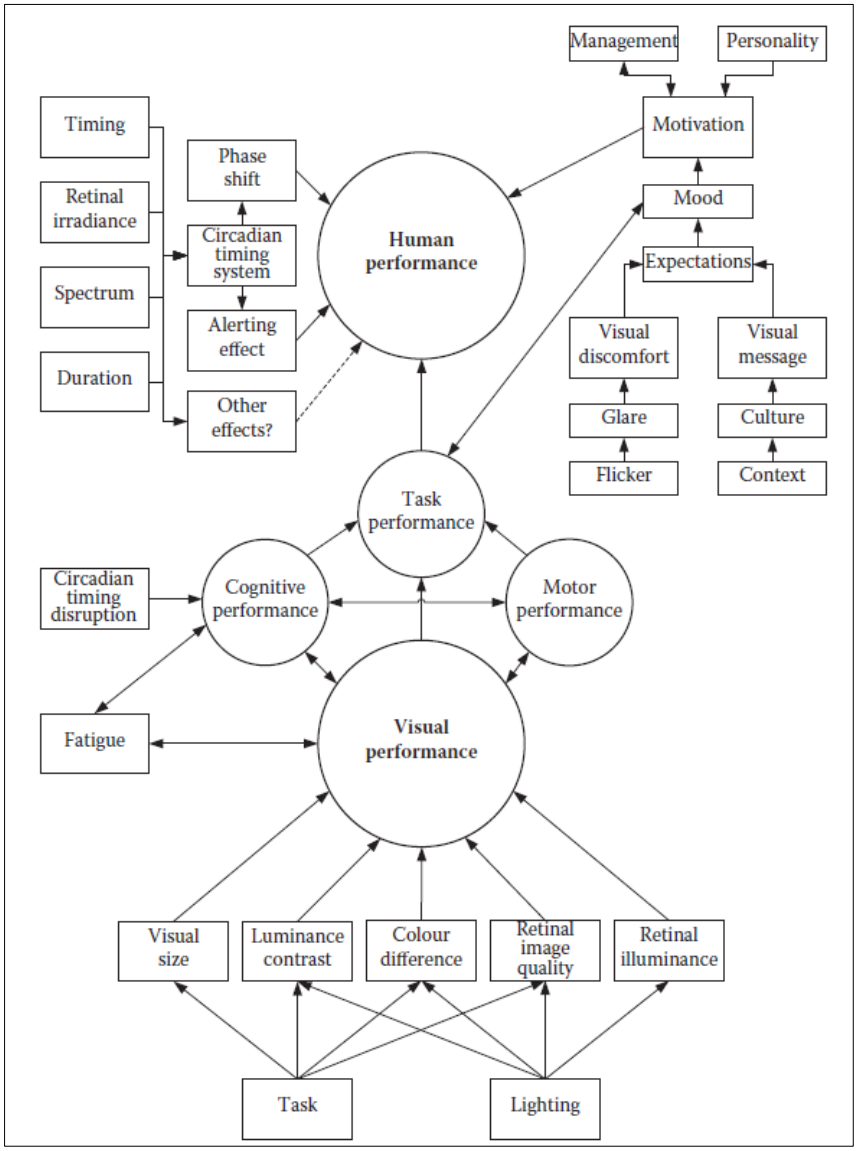

Figure 5 A conceptual framework setting out the three routes whereby lighting conditions can influence human performance. The arrows in the diagram indicate the direction of effect.

To understand how lighting affects work performance, it is essential to identify the three main pathways through which lighting influences human performance: the visual system, the circadian timing system, and mood and motivation. Figure 5 presents a conceptual framework that outlines the factors affecting these pathways and their interactions.

The most apparent effect of lighting on humans is through vision. Light enables us to see, whereas its absence renders us blind. The visual system functions as an image-processing system. The eye's optics create an image of the external environment on the retina, where some initial processing takes place. Various components of the retinal image are processed by different channels as the information travels to the visual cortex in the brain. The magnocellular

channel processes information quickly but with limited detail and no colour, while the parvocellular and koniocellular channels handle details related to brightness, colour, and texture but at a slower pace.

The visual system is also spatially organized into two regions: the fovea, which provides fine detail, and the periphery, which acts as a detection system, guiding the fovea to specific areas of the visual field. Under bright conditions, such as during the day, the entire retina is active. However, in low light conditions, like on a moonless night, the fovea becomes non-functional, and only the peripheral retina remains active.

Any visual stimulus can be characterized by five key parameters: visual size, luminance contrast, colour difference, retinal image quality, and retinal illuminance. These parameters are crucial in determining how effectively the visual system can detect and recognize the stimulus.

2.4 Visual Acuity:

Acuity refers to the ability to resolve fine details, which is ultimately constrained by factors like diffraction, optical aberrations, and the density of photoreceptors in the retina. There are various types of acuity, each corresponding to different levels of visual perception, ranging from basic detection to more complex recognition.

Types of Acuity-

- **Resolution Acuity**: This type of acuity is the ability to perceive two separate stimuli in the visual field as distinct entities, rather than as a single stimulus. It is measured by the smallest angular separation between two stimuli that can still be distinguished, such as the separation between two stars at night. Resolution acuity typically measures around 1 minute of arc.
- **Recognition Acuity**: This refers to the ability to correctly identify a visual target, such as distinguishing between similar letters like "G" and "C." Recognition acuity is commonly tested in clinical settings using letter charts. It generally measures in the range of a few minutes of arc.
- **Vernier Acuity**: Vernier acuity involves detecting slight misalignments between two lines. It is highly precise and is typically measured in the range of a few seconds of arc.

2.5 Literature Reviews:

Paper title: "*The impact of CCT on driving safety in the normal and accident situation: A VR-based experimental study"*

Authors: ***Xiaojun Li, Jiaxin Ling, Yi Shen, Tong Lu, Shouzhong Feng, Hehua Zhu***

Publication details: ***Advanced Engineering Informatics 50 (2021) 101379***

Review:

Co-related colour temperature (CCT) plays a crucial role in the ensurement of driving safety which influences visual and non-visual performance but it remains unclear about the influence and impact of CCT on visual (reaction time) and non-visual performance (driver fatigue) of the subjects (N=30) who are performing driving tasks under normal and accident situation using a virtual reality experimental setup of a tunnel simulation. Higher value of CCT shows improvement of visual performance. Driving fatigue was an unavoidable consequence when driving towards the centre of the tunnel, as evidenced by this discovery. Along with the help of VR based framework using Unity3D, data analysis and data collection are done through application layer, data layer and physical layer as CCT values are used to map and texture the visual environment of the tunnel. In this paper the analyzation of the impact of CCT on drivers under normal and accident situation where physical, behavioural and face validities were studied. The effect of CCT, CRI and other behavioural and biological studies can the done through an AR-VR simulation setup to understand the driving safety overall.

Paper title*: "Project starline: a high-fidelity telepresence system"*

Authors: ***Jason Lawrence, Danb Goldman, Supreeth Achar, Gregory Major Blascovich, Joseph G. Desloge, Tommy Fortes, Eric M. Gomez, Sascha Häberling, Hugues Hoppe, Andy Huibers, Claude Knaus, Brian Kuschak, Ricardo Martin Brualla, Harrisnover, Andrew Ian Russell, Steven M. Seitz, And Kevin Tong***

Publication details: ***ACM Transactions on Graphics Vol 40 (2021) 1–16***

Review:

Telepresence holds an incredible amount of power and opportunities to bring world's increasingly distributed organisations together. A real time fully bidirectional and encumbrance-free 3D communication system that reproduces the experience of being

physically co-present with another person at a distance which enables to feel a strong sense of presence and connectivity.

The main objective of this paper is to capture and render 3D audiovisual likeness for achieving realism, create a comfortable display with retinal resolution, wide field of view stereopsis and motion parallax, lastly to achieve copresence. Incorporation of stereo calculation, 3D face-tracking, compression geometry fusion via ray-casting to achieve overall efficacy of the system and improvement of display architecture and pixel density.

System implementation-The system comprises two main structures: a display unit housing a display, cameras, speakers, microphones, illuminators, and computer, and a backlight unit housing an infrared backlight and also serving as a bench seat. Both units contain white LED strips angled toward the walls and ceiling to produce soft bounce lighting. The capture subsystem consists of three synchronized stereo RGBD capture pods: two above the display, and one in the "middle wall" below the display. The lower pod includes an extra colour camera, zoomed into the subject's face. Four monochrome tracking cameras, two above the display and one on each side, capture high-speed wide-angle images for real-time 3D localization of the eyes, ears, and mouth. The four colour and three depth streams from the RGBD capture pods are compressed on the GPU and transmitted alongside tracked3D face points using WebRTC. On the receiving side, the three depth streams are rendered from the viewer's left and right eye locations using a novel "image-based fusion" ray-casting algorithm. The four colour texture streams are projected onto the fused surface and blended using weights determined from smoothed surface normal.

Here for image-based rendering approach to depict the acquired surface at new views reconstruction of illumination or reflectance models are not done instead, it simply interpolates the textures from the four colour cameras. A drawback is that surfaces with non-Lambertian (e.g., specular) reflectance are rendered incorrectly under non-diffuse lighting and to mitigate this the researchers have created a soft lighting environment using indirect bounce sources. On the sides and back of the display and backlight units, white LED light strips illuminate the surrounding walls, producing a pleasing diffuse source that minimizes sharp highlights. This spread-out light is also more comfortable for the user than direct illumination by the bright LEDs.

Furthermore, a controlled, within-subjects experiment has been conducted wherein each participant (N=25) engaged in a 5 minutes conversation using both systems and conventional videoconferencing. This allowed researchers to statistically test for communication variables

and incorporate behavioural measures such as body language and memory recall, in addition to self-report data.

A study of object under different lighting conditions and the effects on human eye and brain, lighting design could be realised with this work.

Paper title: "*Shopping in virtual reality: A literature review and future agenda"*

Authors: ***Nannan Xi, Juho Hamari***

Publication details: ***Journal of Business Research 134 (2021) 37–58***

Review:

Virtual reality is considered as one of technological megatrends progressing the digitisation of all areas of human life. Shopping and retail have been considered as one of the most promising application areas of VR in business context such as retail giants like Amazon, Ikea, have been making effort to embed virtual reality into their e-commerce shopping ecosystem. In this paper it has been found that the sensory modalities provide additional information like sense of sound, touch, smell, visual output etc. VR shopping can be divided into areas of affection, immersion, cognition, attitude, and usability. Generally, consumers can gain positive affective experiences in the VR environment such as enjoyment. Conceptually virtual reality and VR shopping have been touted to provide disruption and paradigm shifts to shopping, as well as to provide new kinds of shopping experiences for consumers. Future research should further investigate on the following areas such as the effectiveness and efficiency of VR shopping, exploration of moderators and gaining an in-depth understanding boundary conditions ,role of shoppers in VR shopping by studying the biological data sets via different sensors and tracking devices where physiological indices can provide behavioural study of consumers, Ergonomic considerations VR devices where more advanced, lightweight HMD(head-mounted device) in order to provide efficiency and comfort for the consumer's activity, Cybersickness issue induced by VR which are nausea ,oculomotor issues disorientation etc., Therefore, future analysts should think about implementing more standard and essential intelligence with the objects and the surroundings in the simulated virtual shopping environment. Examples of this include developing programmes that turn, move, touch, drop, pick, and shake intuitively, as well as employing increasingly sophisticated and multifunctional intuitive devices, Expansion of movement space with aid of treadmill, technologies like taste and smell sensors, auditory output devices, and haptic devices which vibrate, exert forces, or imitate motion in order to replicate more sensory

experiences. In general, our perception of the outside world is multimodal by nature, frequently incorporating stimuli that are visual, aural, tactile, olfactory, gustatory, and, occasionally, nociceptive simulation. The research extends to various aspects of agility and effectiveness and the factors that influence them in virtual reality shopping environments.

Paper title: "*The virtualization of human–robot interactions: a user-centric workload assessment"*

Authors: ***Federica Nenna, Valeria Orso, Davide Zanardi, Luciano Gamberini***

Publication details: ***Virtual Reality (2023) 27:553–571***

Review:

This paper explores the use of virtual reality (VR) in human-robot collaboration (HRC) and its impact on performance and workload. It discusses the potential benefits of VR simulations for training and familiarizing operators with robotic arms in industrial settings. The study involved participants performing a pick-and-place task and an arithmetic task in both virtual and physical conditions. Performance data was analysed using generalized linear models (GLMs), and pupil size variations were analysed using generalized additive mixed models (GAMMs) and linear mixed-effects models (LMERs). The experimental sample consisted of 21 participants (5 women and 16 men) with normal or corrected-to-normal visual acuity and no neurological or psychiatric problems. The participants underwent a training session and then performed tasks in both virtual and physical conditions. The tasks included a pick-and-place task and an arithmetic task. The order of the conditions was counterbalanced among the participants. After each task, participants filled in the NASA-TLX questionnaires. The results showed that VR simulations can improve performance in HRC tasks, with participants achieving similar learning outcomes compared to standard training methods. The use of VR also reduced mental workload, as indicated by pupil size variations. However, some procedural differences between the virtual and physical conditions were noted. The findings suggest that VR simulations can be effective in training operators for HRC tasks and reducing mental workload. However, the study acknowledges the need for highly immersive and advanced virtual devices for large-scale implementation in industrial settings. The limitations of the study include differences in eye-tracking systems and the use of a relatively inexperienced sample. The paper concludes by highlighting the implications of the findings for the industrial domain and suggesting potential future research directions.

Paper title: "*An Integrated VR/MR Framework for User-Centric Interactive Experience of Cultural Heritage: The ArkaeVision project.*"

Authors: ***Guido Bozzelli, Antonio Raia, Stefano Ricciardi, Maurizio De Nino, Nicola Barile, Marco Perrella, Marco Tramontano, Alfonsina Pagano, Augusto Palombini***

Publication details: ***Digital Applications in Archaeology and Cultural Heritage (2019) Vol 24 e00124***

Review:

The ArkaeVision project aims to create an immersive VR/AR experience for users to interact with cultural heritage, combining storytelling, VR, and AR elements for high-quality 3D graphics and cultural content. The project focuses on providing a user-centric interactive approach, allowing customization for different user profiles and scalability for various cultural sites. It aims to enhance the traditional museum experience by reconstructing damaged cultural objects through virtuality and providing emotional and involving insights into their stories.

The full Platform includes a web portal, an application in Virtual reality and an application in augmented reality. ArkaeVision is deployed from two contexts of two different technologies which are- ArkaeVision Archeo, an experience made with a dedicated HMD related to the Temple of Hera II of Paestum as main subject; it uses the VR, where the actual scenario overlaps and integrates itself with the 3D reconstruction of the archaeological site. ArkaeVision Art, an experience in Augmented Reality (AR) made by using a mobile or a tablet, related to the Tomb of the diver of Paestum as main subject; the AR is used to animate the scenes represented in the various slabs of the tomb

The architecture of ArkaeVision platform is organized in five layers. User layer: it refers to all possible addresses of the platform that are common user, system administrator, local operator;

● Hardware layer: it includes all the hardware devices used by the platform;

● Interface layer (or low-level layer): it represents the drivers to communicate with the hardware;

● Manager layer (or medium level layer): it consists of all the modules dedicated to the management;

● Decision Making layer (or high-level layer): it is really depending by the specific application and includes the application logic and the Artificial Intelligence library.

Each layer includes one or more modules that can communicate with others using an event-based system. This means that every action, gesture, and decision made by the end-user it will be tracked and put in relation with the game logic and the narrative. Technically, each module can be performed by one or more plug-in and it provides at least one. This project also incorporates motion capture (mocap) technology to achieve believable animation of body and face. This involves using high-speed capture cameras and IR-reflective markers on an actress to capture body and facial expressions, which are then blended in real-time by the animation engine. Lighting plays an important role in vision so incorporation of human-centric lighting to this project and also the inclusion of an updated lighting sensors could be a future scope of this work.

Paper title: "*Visionary VR: An Optical Simulation Tool for Evaluating and Optimizing Vision Correction Solutions in Virtual Reality"*

Authors: ***Benedikt W. Hosp, Martin Dechant, Yannick Sauer, Bjorn Severitt, Rajat Agarwala and SiegfriedWahl***

Publication details: ***Sensors (2024), Vol 24, Page 2458***

Review:

In the evolving field of vision science, conventional research methods often fall short in accurately simulating and evaluating vision correction techniques, leading to lengthy and restrictive evaluations. To address these issues, we present 'Visionary VR,' a virtual reality (VR) simulation framework designed to improve optical simulation accuracy and expand research capabilities. Visionary VR utilizes an adaptable VR environment to accommodate dynamic vision tasks and includes comprehensive eye-tracking features. The experiment manager's scene-loading capability provides a scalable and flexible research platform. Initial validation through an empirical study has shown Visionary VR's effectiveness in replicating various visual impairments and assessing vision correction solutions effectively. The results highlight a notable enhancement in evaluating vision correction methods and user experience, demonstrating Visionary VR's potential to revolutionize vision science research by bridging theoretical concepts with practical applications. This validation confirms Visionary VR's role in overcoming traditional methodological limitations and establishing a robust foundation for innovation in vision science research.

CHAPTER 3

3.1 A Landolt's based experimental design for abstract studies in connection with human-centric lighting:

Vision, which is the most complex of our senses, is arguably the most crucial mechanism for perceiving the world around us. It emerges from the intricate interaction between the eye and the brain. Through vision, we form perceptions, and from these perceptions, we construct our individual realities, all of which are significantly influenced by the luminous environment. Understanding this process is essential for designing environments that support optimal visual experiences. Viewing the eye and brain as a unified system offers the best approach to comprehending the biological mechanisms that enable vision.

The Landolt C, also referred to as a Landolt ring, Landolt broken ring, or Japanese vision test, is a standardized symbol used in vision testing, known as an optotype, developed by Swiss ophthalmologist Edmund Landolt in the late 19th century, this symbol consists of a ring with a gap, resembling the letter "C." The Landolt ring test consists of a series of rings, each with a gap oriented in one of the four cardinal directions such as left, right, top, bottom, or at 45 degree angles. The key aspect of the Landolt ring is this gap. The gap's angular size determines the critical detail, while the critical contrast refers to the luminance contrast between the ring and its background. One practical advantage of using the Landolt ring chart as a standard vision test is its versatility; it can be reproduced in large quantities across various media, with the gap size and contrast easily adjustable. The task for the person being tested is to identify the direction of the gap. As the test progresses, the size of the ring and its gap gradually decreases until the person reaches a specified error rate. The smallest angle at which the gap can still be detected is used to measure visual acuity. Commonly used in laboratory settings, the Landolt C has become a standard tool in ophthalmology and vision research for its effectiveness in accurately assessing visual sharpness.

The experiment is designed to investigate how varying correlated colour temperatures (CCTs) influence visual acuity and physiological responses. By utilizing EEG and galvanic skin response (GSR) measurements, the study aims to assess the effects of different lighting conditions on both visual performance and physiological reactions in real time, as well as to validate these findings in a simulated virtual reality environment.

3.1.1 Experimental setup and procedure:

3.1.1.1 *Participants*- Five participants (n=5), all postgraduate students from Jadavpur University's Electrical Engineering department with normal or corrected to normal vision, participated in the study. They were fully briefed on the task and gave their consent before the experiment. All the participants were university postgraduate students, with ages ranging from 24 to 27 years. The study included 4male participants and 1 female participant, with an average age of 25.5 years.

3.1.1.2 *Experimental design*- The experiment involves using Landolt rings to assess the effect of different correlated colour temperatures (CCTs) on visual performance. Each Landolt ring has a height of 1 cm and a gap of 0.2 cm, and they are printed on a 14x10 matrix sheet, totalling 140 rings per sheet. The study examines four CCT variations: 3000K, 4000K, 5000K, and 6000K. To minimize bias, the placement of the Landolt rings varies for each CCT condition. Participants are tasked with identifying the Landolt C rings with a gap on the right side. Each chart contains 40 Landolt C rings, and there are no time constraints, as the test is participant-driven test.

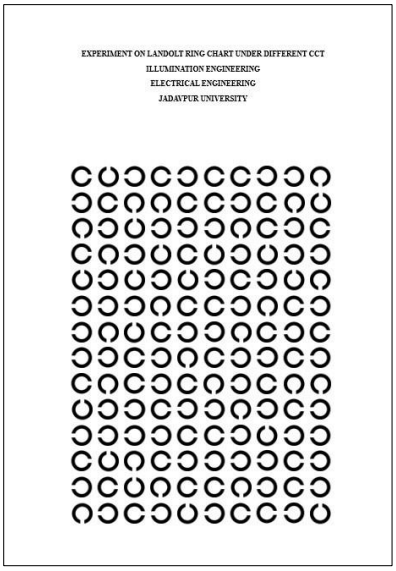

Figure 6 Landolt ring chart

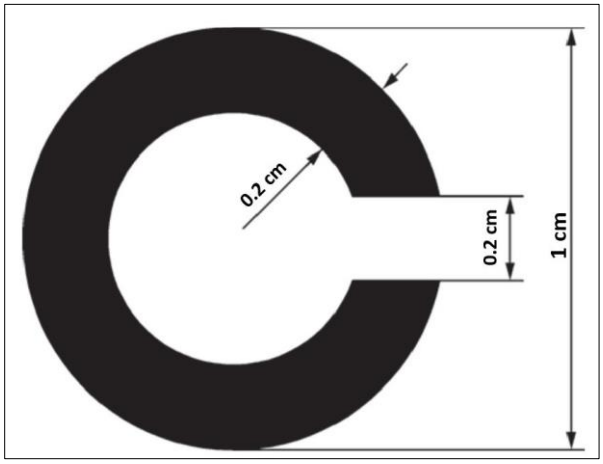

Figure 7 A visualisation of the Landolt ring featuring the gap(0.2cm) and the symbol's height(1cm).

3.1.1.3 *Experimental setup*- The experiment was conducted in the Illumination Engineering Laboratory within the Department of Electrical Engineering, Jadavpur University. To investigate the effects of correlated colour temperature (CCT) on neurocognitive and behavioural performance, a Wi-Fi enabled, dimmable, CCT controllable 12-watt LED light

source subtended at height of 1 m from the working plane. To prevent direct light from entering the observer's eyes and to improve visual comfort and clarity, a black conical-shaped paper was used as a baffle around the light source, thus reducing the distraction of excessive brightness. The dimension of the working plane is 8m x 6m. Forty-eight grid points were marked on the working plane, spaced 0.5 meters apart, with rows labelled A to H and columns numbered 1 to 6. In accordance with IS 3646 standards, the nadir point on the working plane is located at E4.

3.1.1.4 *Experimental procedure*- Four different CCT settings—3000K, 4000K, 5000K, and 6000K were examined and the CCT values were verified using a Calorimeter CL-70F. The light source was initially set to 100% intensity and connected to Wi-Fi for CCT control. Lux levels at each grid point on the working plane were measured with a lux meter. Neurocognitive and behavioural performance under varying CCTs was assessed using EEG and GSR. In the Landolt ring task, participants identified rings with gaps oriented to the right. The time taken and errors made under each lighting condition were recorded, alongside EEG and GSR data to monitor neural and electrodermal activity.

3.1.1.5 *Data recording*- Twenty sets of data were collected from the experiment, as five participants performed tasks under four different CCTs. Initially, a 2-minute conditioning period was conducted, with participants spending one minute with their eyes closed and one minute with their eyes open. Following the conditioning phase, the task commenced. Two key events were marked in the EEG recordings: one at the start of the task and another at the end. These markers were used to calculate the reaction time of the participants. Data from EEG, GSR, and the simulation output were gathered for further analysis.

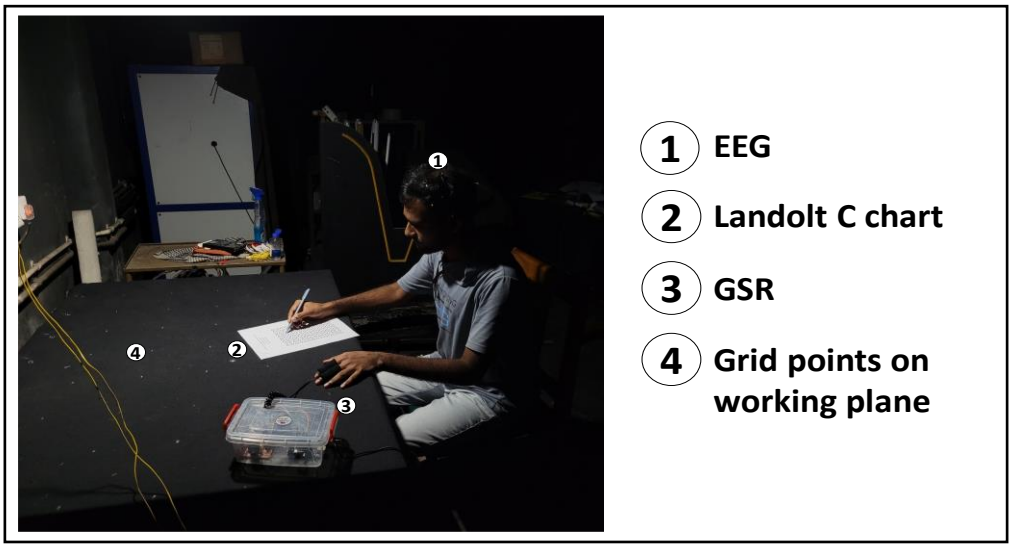

Figure 8 Landolt C ring experiment in progress

3.2 A Landolt's based virtually simulated experimental design in connection with human-centric lighting:

The aim of this experiment is to replicate the Landolt's experiment performed previously in real time and the validation of the same in a virtually simulated environment by using EEG and to tally out the data and to establish that virtual reality is a powerful and valid tool for human centric lighting research purposes.

3.2.1 Experimental setup and procedure:

3.2.1.1 *Participants*- Five participants (n=5), all postgraduate students from Jadavpur University's Electrical Engineering department with normal or corrected to normal vision, participated in the study. They were fully briefed on the task and gave their consent before the experiment. All the participants were university postgraduate students, with ages ranging from 24 to 27 years. The study included 4 male participants and 1 female participant, with an average age of 25.5 years.

3.2.1.2 *Experimental design*- To validate the experiment, an exact replication of the real-time experiment discussed in the previous chapter was developed in Unity using the High Definition Render Pipeline (HDRP) version. Initially, the Landolt C charts from the real-time experiment were precisely recreated and coded in C# using Unity's code editor, Microsoft Visual Studio Code. In the code, the directions of the gap in the Landolt C were represented as 90 degrees, -90 degrees, 180 degrees, and 0 degrees, corresponding to the gap being oriented up, down, left, and right, respectively. To accurately simulate the lighting conditions, the photometric properties of an LED light source were implemented by importing its IES file into the Unity project. As the experiment involves four variations of CCT—3000K, 4000K, 5000K, and 6000K—the Landolt C charts were numbered 1, 2, 3, and 4 accordingly. For instance, when the 3000K CCT is applied, chart number 1 is displayed. During the experiment, users must select the correct Landolt C, and the system records the selection time, the position of the Landolt C (indicated by row and column in the matrix), and outputs this data for analysis.

3.2.1.3 *Experimental setup*- The experiment was performed in illumination engineering lab in the department of electrical engineering, Jadavpur university. At first the EEG device was placed onto the scalp of the participant meticulously following the 10-20 system by placing the electrodes at the correct points. Then the VR set meta quest 2 through which the VR simulation

is seen set onto the participants accordingly to their comfort. Then GSR electrodes are worn on the left hand specifically on the index and middle finger.

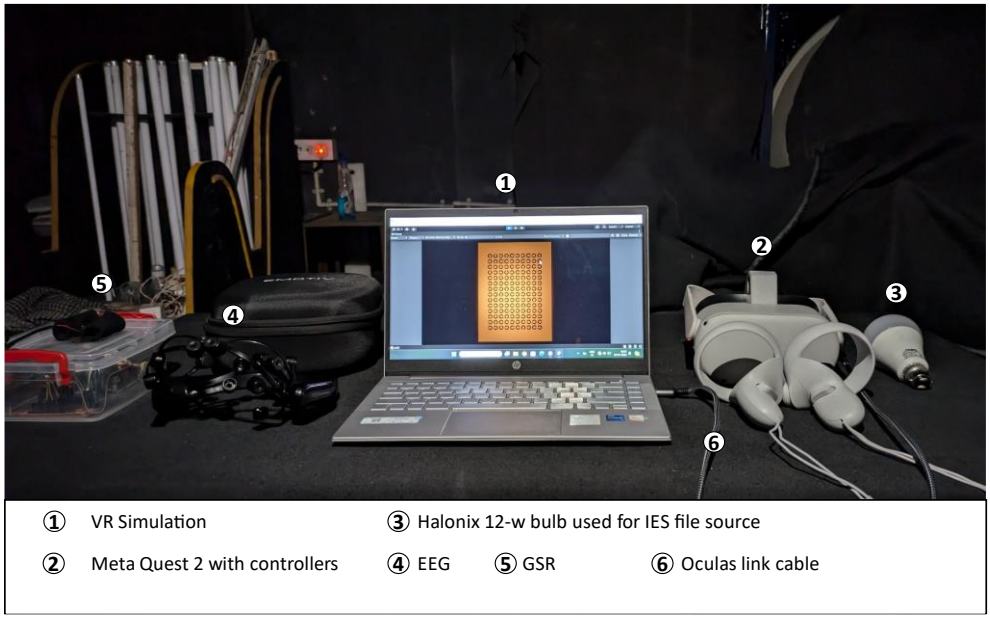

Figure 9 Landolt C ring VR experimental setup

3.1.1.4 *Data recording*- Twenty sets of data were collected from the experiment, as five participants performed tasks under four different CCTs. Initially, a 2-minute conditioning period was conducted, with participants spending one minute with their eyes closed and one minute with their eyes open. Following the conditioning phase, the task commenced. Two key events were marked in the EEG recordings: one at the start of the task and another at the end. These markers were used to calculate the reaction time of the participants. Data from EEG, GSR, and the simulation output were gathered for further analysis.

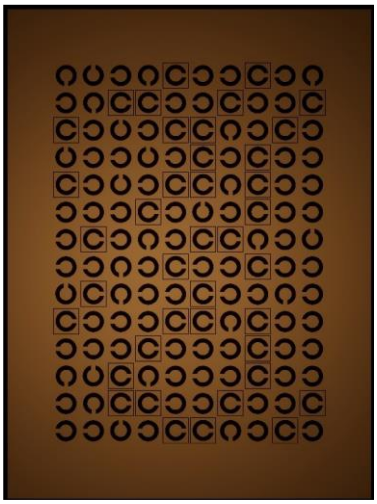

Figure 10 Landolt C ring VR simulation under 3000K

Figure 11 Participant undergoing Landolt C ring VR experiment.

3.3 Experimental Workflow:

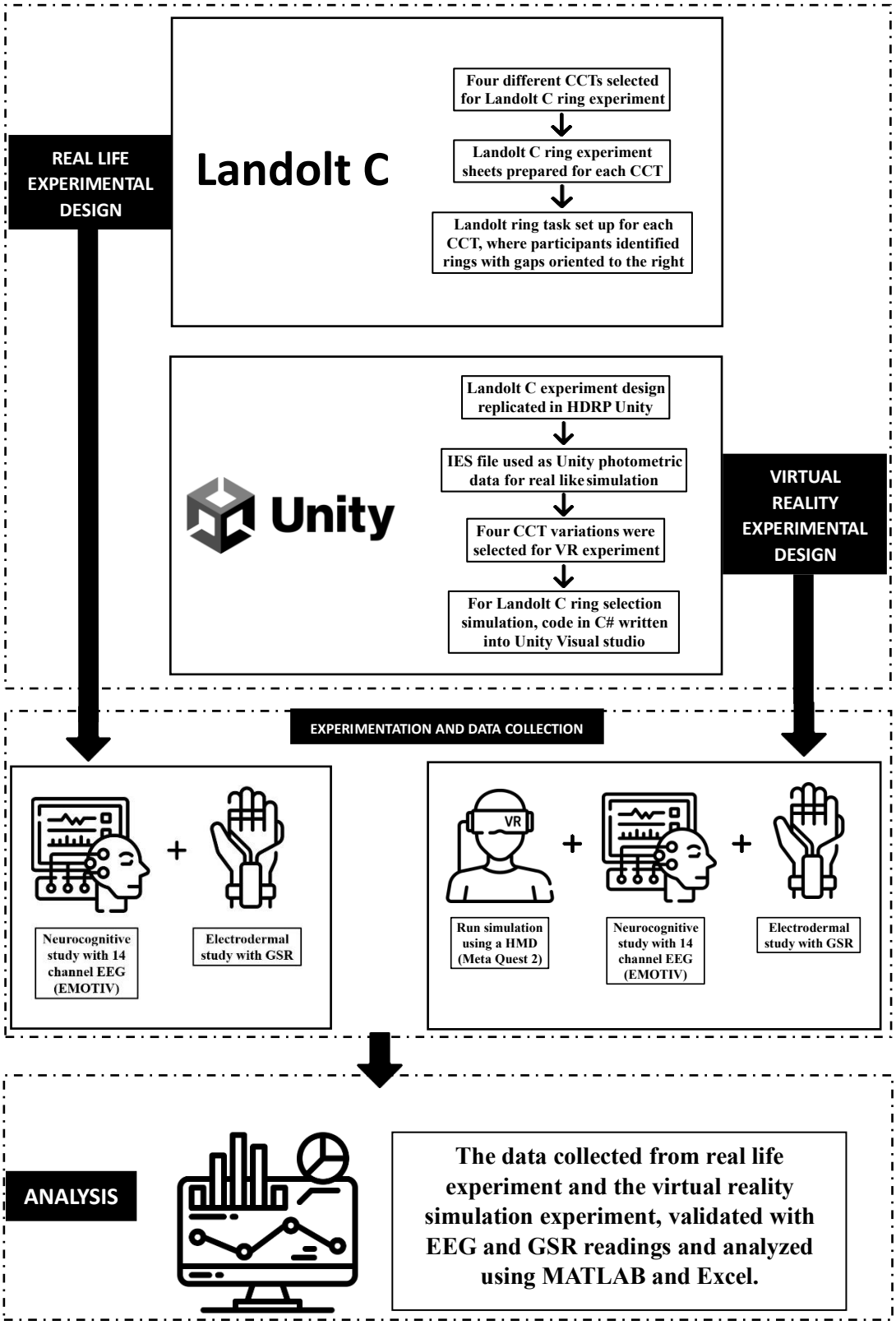

CHAPTER 4

4.1 Experimental Results:

```
{index = Row : 0 Col : 4}, {rotation = 0}, {time = 24.5720767}
{index = Row : 0 Col : 7}, {rotation = 0}, {time = 30.0848677}
{index = Row : 1 Col : 2}, {rotation = 0}, {time = 37.8820283}
{index = Row : 1 Col : 3}, {rotation = 0}, {time = 43.6653545}
{index = Row : 1 Col : 6}, {rotation = 0}, {time = 46.7751613}
{index = Row : 1 Col : 9}, {rotation = 0}, {time = 50.9624323}
{index = Row : 2 Col : 0}, {rotation = 0}, {time = 54.542648}
{index = Row : 2 Col : 4}, {rotation = 0}, {time = 60.1918784}
{index = Row : 2 Col : 5}, {rotation = 0}, {time = 62.5187853}
{index = Row : 2 Col : 8}, {rotation = 0}, {time = 65.9824833}
{index = Row : 3 Col : 5}, {rotation = 0}, {time = 74.4814905}
{index = Row : 3 Col : 7}, {rotation = 0}, {time = 77.3118617}
{index = Row : 4 Col : 0}, {rotation = 0}, {time = 82.7656062}
{index = Row : 4 Col : 4}, {rotation = 0}, {time = 87.9836858}
{index = Row : 4 Col : 5}, {rotation = 0}, {time = 89.8314369}
{index = Row : 4 Col : 7}, {rotation = 0}, {time = 92.4149251}
{index = Row : 5 Col : 3}, {rotation = 0}, {time = 100.0393847}
{index = Row : 5 Col : 7}, {rotation = 0}, {time = 106.3112891}
{index = Row : 6 Col : 1}, {rotation = 0}, {time = 111.7391526}
{index = Row : 6 Col : 5}, {rotation = 0}, {time = 116.552942}
{index = Row : 6 Col : 6}, {rotation = 0}, {time = 118.8954158}
{index = Row : 7 Col : 4}, {rotation = 0}, {time = 128.5458743}
{index = Row : 7 Col : 7}, {rotation = 0}, {time = 132.7376555}
{index = Row : 8 Col : 1}, {rotation = 0}, {time = 140.2612711}
{index = Row : 8 Col : 5}, {rotation = 0}, {time = 145.1875838}
{index = Row : 9 Col : 0}, {rotation = 0}, {time = 151.9915658}
{index = Row : 9 Col : 4}, {rotation = 0}, {time = 158.7780992}
{index = Row : 9 Col : 5}, {rotation = 0}, {time = 160.9726406}
{index = Row : 9 Col : 7}, {rotation = 0}, {time = 163.5760767}
{index = Row : 10 Col : 3}, {rotation = 0}, {time = 176.1725271}
{index = Row : 10 Col : 7}, {rotation = 0}, {time = 181.2126763}
{index = Row : 11 Col : 2}, {rotation = 0}, {time = 187.4927418}
{index = Row : 11 Col : 7}, {rotation = 0}, {time = 196.7478555}
{index = Row : 12 Col : 2}, {rotation = 0}, {time = 203.9905228}
{index = Row : 12 Col : 3}, {rotation = 0}, {time = 208.0595437}
{index = Row : 12 Col : 6}, {rotation = 0}, {time = 211.3898587}
{index = Row : 13 Col : 4}, {rotation = 0}, {time = 220.0310791}
{index = Row : 13 Col : 5}, {rotation = 0}, {time = 222.2469582}
{index = Row : 13 Col : 8}, {rotation = 0}, {time = 227.6543588}
```

Figure 12 Output of a subject under 3000K in VR simulation

```
{index = Row : 0 Col : 5}, {rotation = 0}, {time = 15.9711152}
{index = Row : 0 Col : 9}, {rotation = 0}, {time = 19.1330161}
{index = Row : 1 Col : 0}, {rotation = 0}, {time = 23.0033083}
{index = Row : 1 Col : 4}, {rotation = 0}, {time = 25.7557344}
{index = Row : 1 Col : 5}, {rotation = 0}, {time = 28.8359492}
{index = Row : 1 Col : 6}, {rotation = 0}, {time = 30.7158466}
{index = Row : 2 Col : 5}, {rotation = 0}, {time = 37.2369735}
{index = Row : 2 Col : 7}, {rotation = 0}, {time = 39.4974219}
{index = Row : 2 Col : 9}, {rotation = 0}, {time = 41.0692496}
{index = Row : 3 Col : 5}, {rotation = 0}, {time = 45.2181737}
{index = Row : 3 Col : 7}, {rotation = 0}, {time = 47.2288918}
{index = Row : 4 Col : 2}, {rotation = 0}, {time = 51.96669}
{index = Row : 4 Col : 3}, {rotation = 0}, {time = 53.6363221}
{index = Row : 4 Col : 5}, {rotation = 0}, {time = 55.9932178}
{index = Row : 4 Col : 9}, {rotation = 0}, {time = 59.0472243}
{index = Row : 5 Col : 1}, {rotation = 0}, {time = 62.304736}
{index = Row : 5 Col : 4}, {rotation = 0}, {time = 65.0036256}
{index = Row : 5 Col : 7}, {rotation = 0}, {time = 68.1732477}
{index = Row : 6 Col : 2}, {rotation = 0}, {time = 72.9393425}
{index = Row : 6 Col : 5}, {rotation = 0}, {time = 75.8914995}
{index = Row : 6 Col : 8}, {rotation = 0}, {time = 78.2811091}
{index = Row : 7 Col : 0}, {rotation = 0}, {time = 81.8819369}
{index = Row : 7 Col : 4}, {rotation = 0}, {time = 86.1853367}
{index = Row : 7 Col : 9}, {rotation = 0}, {time = 90.0570138}
{index = Row : 8 Col : 3}, {rotation = 0}, {time = 95.3849045}
{index = Row : 8 Col : 9}, {rotation = 0}, {time = 99.8146604}
{index = Row : 9 Col : 1}, {rotation = 0}, {time = 103.0933144}
{index = Row : 9 Col : 2}, {rotation = 0}, {time = 105.3411439}
{index = Row : 9 Col : 8}, {rotation = 0}, {time = 109.5481234}
{index = Row : 10 Col : 3}, {rotation = 0}, {time = 113.5584879}
{index = Row : 10 Col : 9}, {rotation = 0}, {time = 117.778342}
{index = Row : 11 Col : 6}, {rotation = 0}, {time = 125.052348}
{index = Row : 11 Col : 7}, {rotation = 0}, {time = 127.1946504}
{index = Row : 12 Col : 4}, {rotation = 0}, {time = 133.154975}
{index = Row : 12 Col : 6}, {rotation = 0}, {time = 135.0819275}
{index = Row : 12 Col : 9}, {rotation = 0}, {time = 137.4696133}
{index = Row : 13 Col : 3}, {rotation = 0}, {time = 141.2390775}
{index = Row : 13 Col : 9}, {rotation = 0}, {time = 145.0411835}
```

Figure 13 Output of a subject under 4000K in VR simulation

```
{index = Row : 0 Col : 2}, {rotation = 180}, {time = 14.7368106}
{index = Row : 0 Col : 3}, {rotation = 0}, {time = 17.4627538}
{index = Row : 0 Col : 6}, {rotation = 0}, {time = 20.7974947}
{index = Row : 1 Col : 0}, {rotation = 0}, {time = 30.3059974}
{index = Row : 1 Col : 1}, {rotation = -90}, {time = 32.7568289}
{index = Row : 1 Col : 4}, {rotation = 0}, {time = 36.938156}
{index = Row : 1 Col : 5}, {rotation = 0}, {time = 38.7848579}
{index = Row : 1 Col : 7}, {rotation = 0}, {time = 41.8412175}
{index = Row : 2 Col : 1}, {rotation = 0}, {time = 46.2832807}
{index = Row : 2 Col : 3}, {rotation = 0}, {time = 49.5908468}
{index = Row : 2 Col : 7}, {rotation = 0}, {time = 53.2523571}
{index = Row : 2 Col : 9}, {rotation = 0}, {time = 55.5846243}
{index = Row : 3 Col : 0}, {rotation = 0}, {time = 59.6174891}
{index = Row : 3 Col : 3}, {rotation = 0}, {time = 64.0573966}
{index = Row : 4 Col : 1}, {rotation = 0}, {time = 74.3979181}
{index = Row : 4 Col : 2}, {rotation = 0}, {time = 76.1121122}
{index = Row : 4 Col : 6}, {rotation = 0}, {time = 79.5587146}
{index = Row : 4 Col : 9}, {rotation = 0}, {time = 82.8484533}
{index = Row : 5 Col : 1}, {rotation = 0}, {time = 86.7746256}
{index = Row : 5 Col : 8}, {rotation = 0}, {time = 99.9013828}
{index = Row : 6 Col : 3}, {rotation = 0}, {time = 112.4537264}
{index = Row : 6 Col : 7}, {rotation = 0}, {time = 119.3225627}
{index = Row : 6 Col : 9}, {rotation = 0}, {time = 122.9263562}
{index = Row : 7 Col : 0}, {rotation = 180}, {time = 129.527459}
{index = Row : 7 Col : 1}, {rotation = 0}, {time = 131.7546526}
{index = Row : 7 Col : 8}, {rotation = 0}, {time = 140.1205225}
{index = Row : 8 Col : 0}, {rotation = 0}, {time = 149.0774829}
{index = Row : 8 Col : 8}, {rotation = 0}, {time = 158.9781103}
{index = Row : 9 Col : 1}, {rotation = 0}, {time = 165.2223832}
{index = Row : 9 Col : 3}, {rotation = 0}, {time = 167.673384}
{index = Row : 9 Col : 8}, {rotation = 0}, {time = 173.8939258}
{index = Row : 9 Col : 9}, {rotation = 0}, {time = 176.2546546}
{index = Row : 10 Col : 1}, {rotation = 180}, {time = 181.0047622}
{index = Row : 11 Col : 0}, {rotation = 0}, {time = 191.5402629}
{index = Row : 12 Col : 0}, {rotation = 0}, {time = 204.7229917}
{index = Row : 12 Col : 4}, {rotation = 0}, {time = 210.7272646}
{index = Row : 12 Col : 5}, {rotation = 0}, {time = 213.8890368}
{index = Row : 12 Col : 8}, {rotation = 0}, {time = 220.2614424}
{index = Row : 13 Col : 0}, {rotation = 180}, {time = 223.8293822}
{index = Row : 13 Col : 1}, {rotation = 180}, {time = 225.9034404}
{index = Row : 13 Col : 7}, {rotation = 0}, {time = 236.8259413}
```

Figure 14 Output of a subject under 5000K in VR simulation

```
{index = Row : 0 Col : 0}, {rotation = 0}, {time = 9.239463}
{index = Row : 0 Col : 3}, {rotation = 0}, {time = 11.9668777}
{index = Row : 0 Col : 5}, {rotation = 0}, {time = 15.454084}
{index = Row : 0 Col : 6}, {rotation = 0}, {time = 17.6348411}
{index = Row : 1 Col : 1}, {rotation = 0}, {time = 22.0318601}
{index = Row : 1 Col : 4}, {rotation = 0}, {time = 24.340961}
{index = Row : 1 Col : 5}, {rotation = 0}, {time = 25.8447045}
{index = Row : 1 Col : 7}, {rotation = 0}, {time = 28.0446798}
{index = Row : 2 Col : 7}, {rotation = 0}, {time = 35.5059677}
{index = Row : 2 Col : 9}, {rotation = 0}, {time = 37.5443674}
{index = Row : 3 Col : 0}, {rotation = 0}, {time = 40.4970146}
{index = Row : 3 Col : 4}, {rotation = 0}, {time = 43.525349}
{index = Row : 4 Col : 6}, {rotation = 0}, {time = 51.8255671}
{index = Row : 5 Col : 4}, {rotation = 0}, {time = 58.6894479}
{index = Row : 5 Col : 5}, {rotation = 0}, {time = 60.4704044}
{index = Row : 5 Col : 8}, {rotation = 0}, {time = 63.6025459}
{index = Row : 6 Col : 3}, {rotation = 0}, {time = 70.3009917}
{index = Row : 6 Col : 7}, {rotation = 0}, {time = 73.7995067}
{index = Row : 6 Col : 9}, {rotation = 0}, {time = 75.9517619}
{index = Row : 7 Col : 2}, {rotation = 0}, {time = 80.1422428}
{index = Row : 7 Col : 5}, {rotation = 0}, {time = 83.1797987}
{index = Row : 7 Col : 8}, {rotation = 0}, {time = 85.8880981}
{index = Row : 8 Col : 0}, {rotation = 0}, {time = 89.591805}
{index = Row : 8 Col : 2}, {rotation = 0}, {time = 91.5003856}
{index = Row : 8 Col : 4}, {rotation = 0}, {time = 93.305836}
{index = Row : 8 Col : 7}, {rotation = 0}, {time = 96.104012}
{index = Row : 9 Col : 3}, {rotation = 0}, {time = 101.9730878}
{index = Row : 9 Col : 8}, {rotation = 0}, {time = 106.8193546}
{index = Row : 10 Col : 4}, {rotation = 0}, {time = 112.8223631}
{index = Row : 10 Col : 5}, {rotation = 0}, {time = 114.2875907}
{index = Row : 11 Col : 0}, {rotation = 0}, {time = 119.3785382}
{index = Row : 11 Col : 3}, {rotation = 0}, {time = 122.769938}
{index = Row : 11 Col : 8}, {rotation = 0}, {time = 125.9335707}
{index = Row : 12 Col : 1}, {rotation = 0}, {time = 129.0174776}
{index = Row : 12 Col : 4}, {rotation = 0}, {time = 131.2366561}
{index = Row : 12 Col : 5}, {rotation = 0}, {time = 132.4806641}
{index = Row : 12 Col : 8}, {rotation = 0}, {time = 134.6270936}
{index = Row : 13 Col : 2}, {rotation = 0}, {time = 138.2829069}
{index = Row : 13 Col : 6}, {rotation = 0}, {time = 141.2347277}
{index = Row : 13 Col : 7}, {rotation = 0}, {time = 142.9256855}
```

Figure 15 Output of a subject under 6000K in VR simulation

The colour of a light source is determined by its spectral composition and the optical power associated with each wavelength. The physical property of light relevant to colour vision is the spectral power distribution (SPD). An SPD specifies the amount of power contained at each wavelength within the visible spectrum, typically ranging from approximately 400 to 700 nm. In practice, spectral power distributions are measured at discrete sample wavelengths, which allow for a detailed characterization of how the light source's power is distributed across different colours.

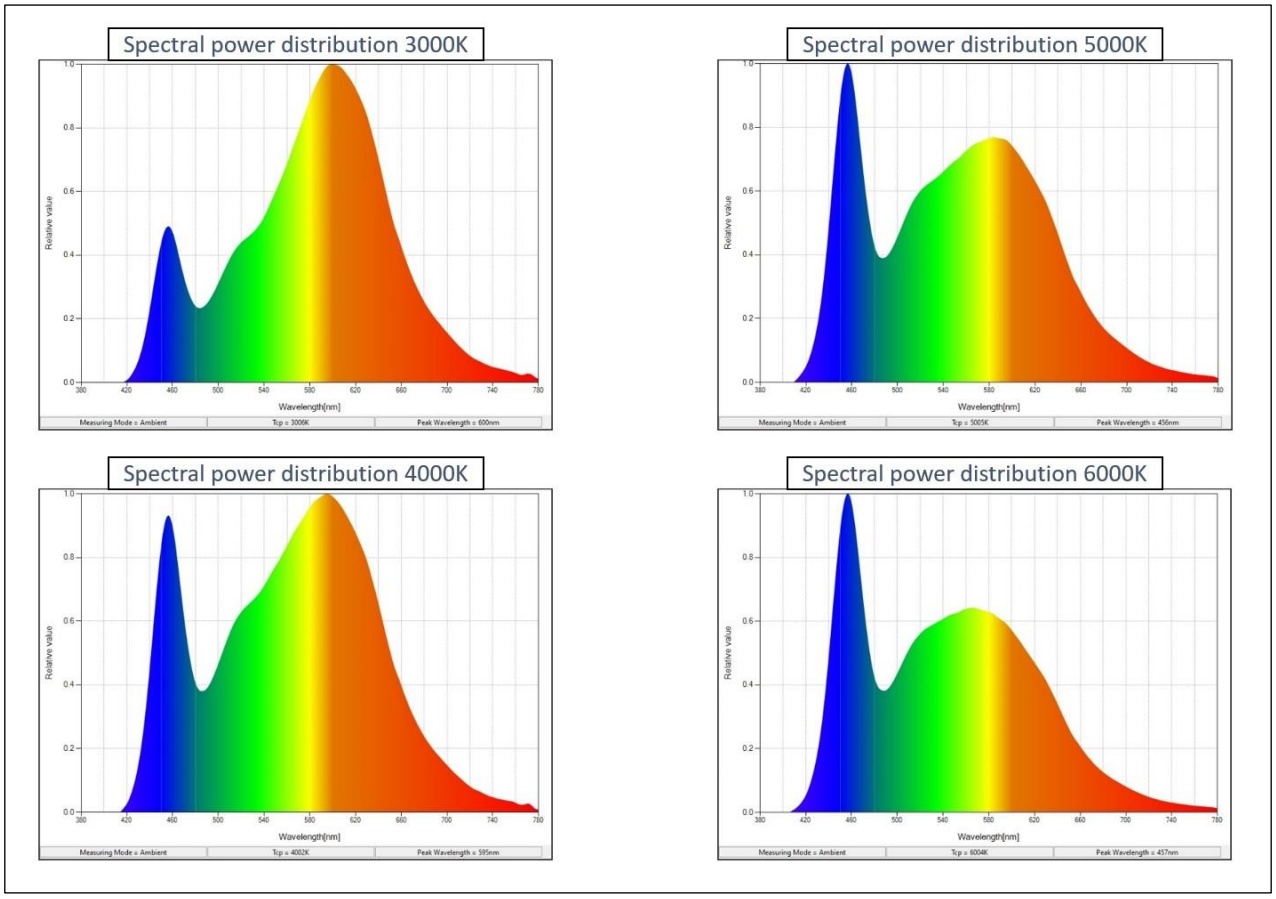

Figure 16 Spectral power distribution of 3000K, 4000K, 5000K and 6000K obtained from CL-70F

CHAPTER 5

5.1 Experimental Analysis:

Table 1 Total number of Landolt C selected by subjects under four CCTs in VR simulated experiment

Subject	3000K	4000K	5000K	6000K
A	40	40	40	40
B	39	38	35	40
C	38	39	39	36
D	40	39	40	40
E	40	39	37	38

Table 2 Total number of Landolt C selected by subjects under four CCTs in real life experiment

Subject	3000K	4000K	5000K	6000K
F	38	39	39	40
G	39	40	40	39
H	40	39	40	39
I	35	36	38	38
J	37	40	37	40

5.2 Galvanic Skin Response (GSR) Analysis:

Electrodermal Activity (EDA), also known as Galvanic Skin Response (GSR), measures changes in the electrical properties of the skin, which vary with emotional arousal and stress. As the body sweats and skin conductance increases under such conditions, EDA is computed by applying a small current between two electrodes placed on the skin and measuring the resulting resistance. The EDA signal comprises two main components: the **Skin Conductance Level (SCL)**, which represents the slow, long-term changes in skin conductance (tonic response), and the **Skin Conductance Responses (SCR)**, which reflect rapid, event-related changes (phasic response). The SCL is used for assessing baseline statistics such as mean and standard deviation, as it provides a stable measurement unaffected by transient peaks. In contrast, the SCR is utilized for detecting immediate arousal responses. EDA, alongside heart rate, is considered a highly effective signal for discriminating between different emotional states and stress levels.

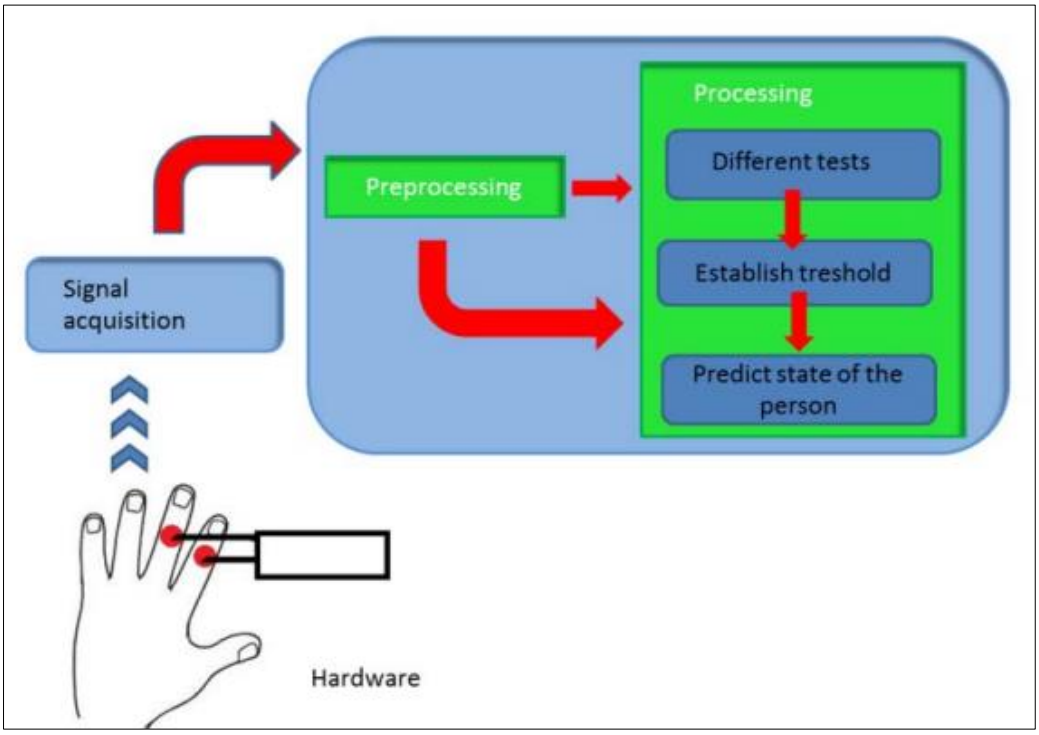

Figure 17 Galvanic Skin Response (GSR) workflow

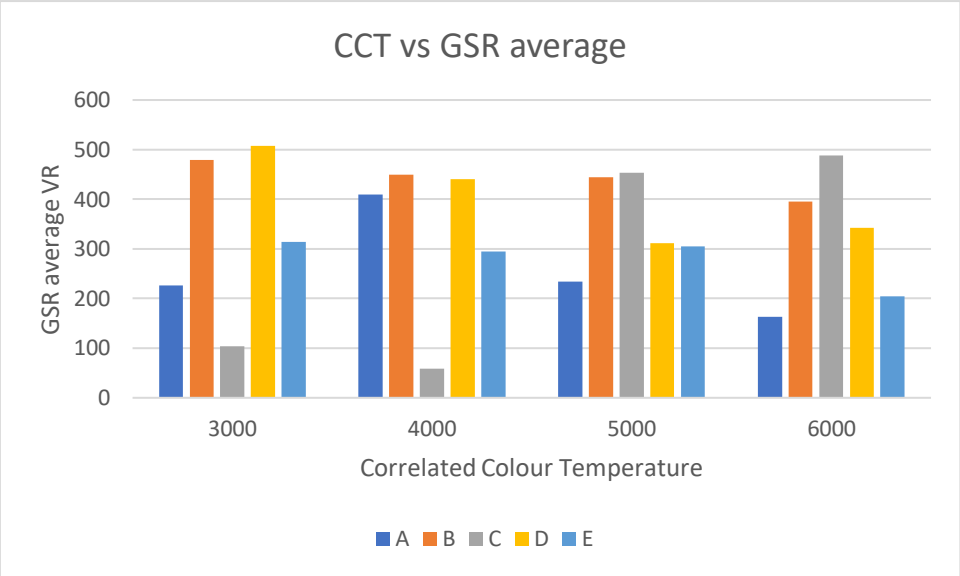

Figure 18a CCT vs GSR average graph for VR experiment

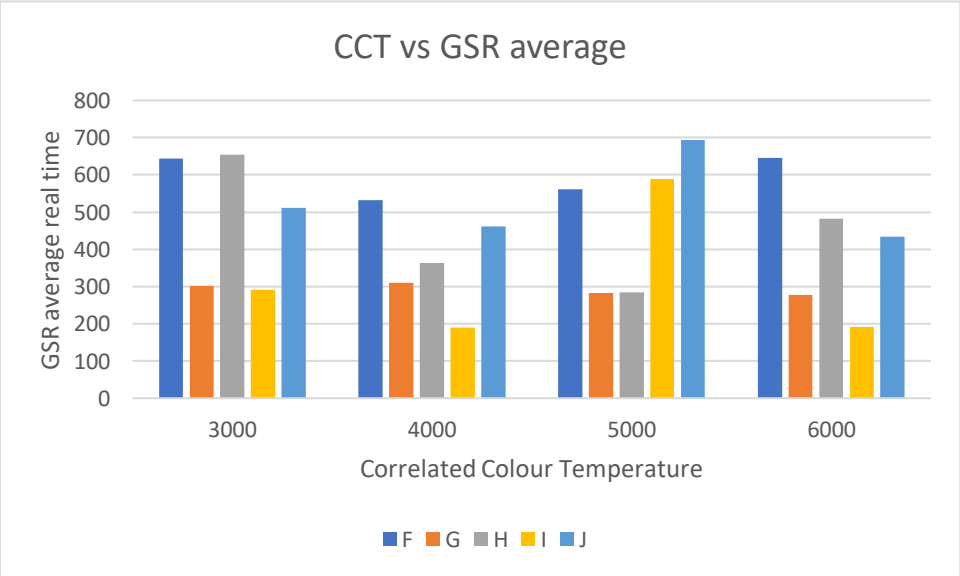

Figure 18b CCT vs GSR average graph for real time experiment

Based on the GSR average plot, it is evident that the electrodermal activity is higher under 5000K and 6000K colour temperatures compared to 3000K and 4000K. This suggests that participants experienced greater emotional arousal or physiological responses under the cooler lighting conditions (5000K and 6000K) than under the warmer ones (3000K and 4000K).

5.3 Electroencephalogram (EEG) Analysis:

The human brain is composed of millions of neurons that play a crucial role in controlling the body's behaviour in response to internal and external motor and sensory stimuli. These neurons act as information carriers, facilitating communication between the brain and the rest of the body. To understand cognitive behaviour, researchers analyse signals or images from the brain, which can provide insights into various motor and sensory states such as eye movement, lip movement, memory recall, attention, and hand clenching. Each of these states is associated with specific signal frequencies, which help to decipher the functional behaviour of the brain's complex structure. Electroencephalography (EEG) is an effective tool for capturing brain signals corresponding to these various states by recording electrical activity from the scalp surface, offering valuable data for understanding brain function

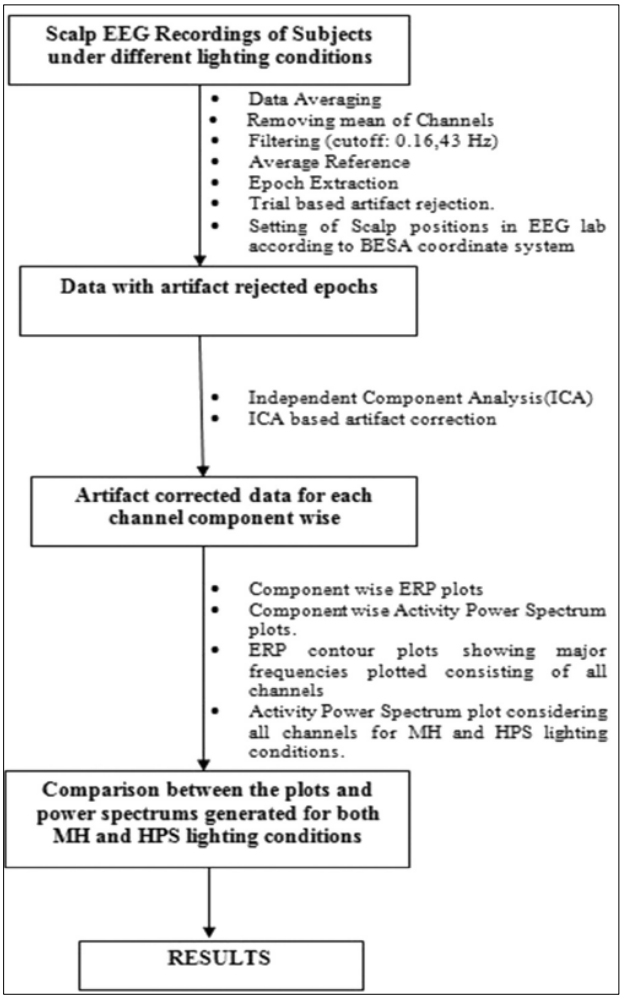

Figure 19 EEG analysis workflow [S. Chakraborty et al.]

Event-related potentials (ERPs) are small electrical voltages in the brain generated in response to specific stimuli, detectable through EEG. They reflect time-locked changes in brain activity associated with sensory, motor, or cognitive events, offering a non-invasive method to study mental processes. ERPs are categorized into **sensory (exogenous)** components, which appear within the first 100 milliseconds of a stimulus and are influenced by its physical properties, and **cognitive (endogenous)** components, which occur later and reflect the brain's evaluative and processing activities. These waveforms are described by their latency (timing) and amplitude (strength), providing valuable insights into how the brain processes and responds to information.

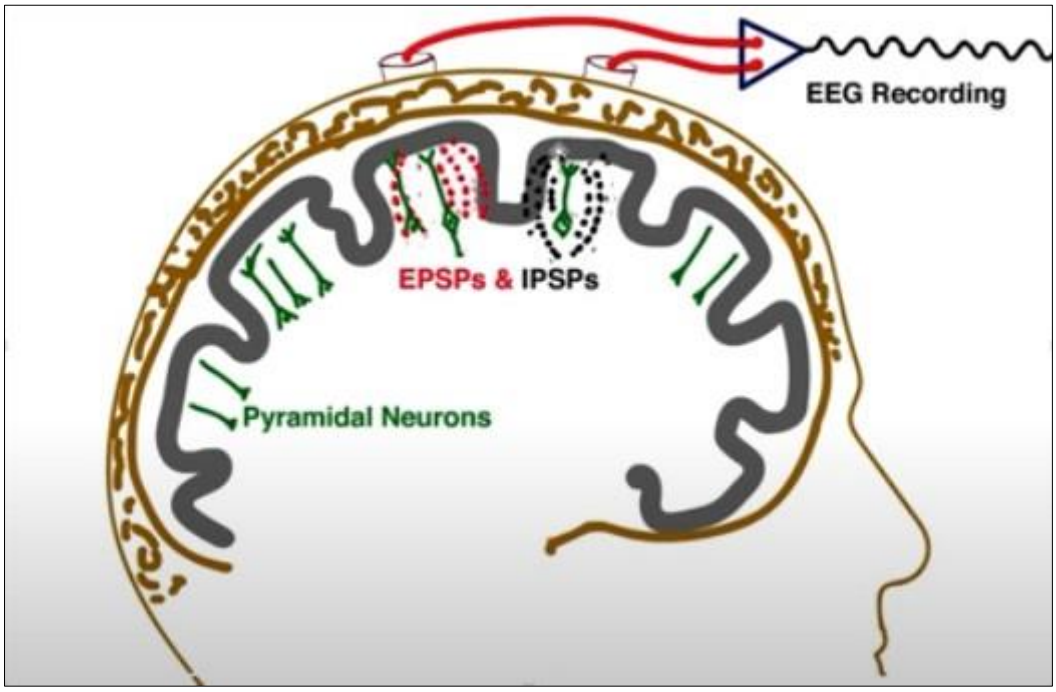

Figure 20 Schematic illustration of Excitatory and Inhibitory Post Synaptic Potential

The 10-20 system, introduced by Herbert Jasper at the 1957 Brussels IV International EEG Congress, was developed to standardize the placement of EEG electrodes on the scalp. The numbers "10" and "20" refer to the distances between adjacent electrodes, which are either 10% or 20% of the total distance across the skull (measured front-to-back or right-to-left). This total distance is determined using key anatomical landmarks on the scalp: the nasion and inion (for the front-to-back direction) and the two preauricular points (for the right-to-left direction).

Based on these landmarks, the electrode positions are determined by applying these specific proportions: the first electrode is placed 10% of the total distance from the anatomical

landmark, and subsequent electrodes are placed 20% apart from one another. For instance, the Fp1 electrode is positioned 10% of the total distance from the nasion, and the Fz electrode is positioned 20% of the distance from Fp1.

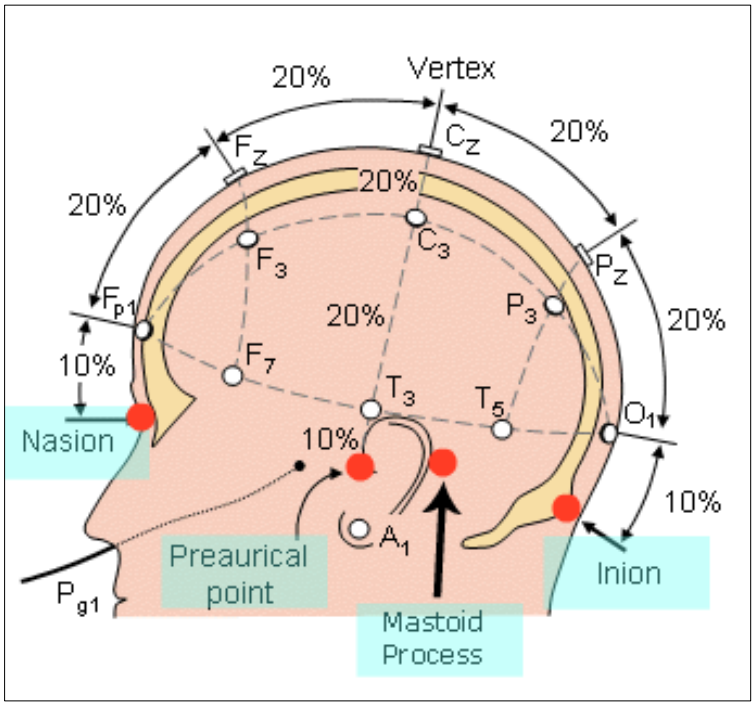

Figure 21 10-20 system of EEG electrode placement

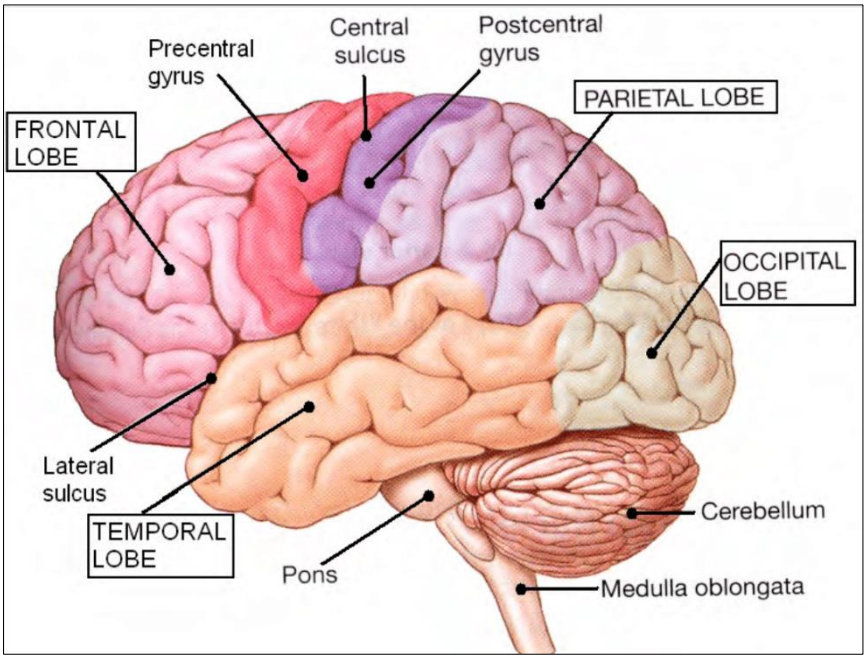

Figure 22 An illustration of human brain anatomical structure

Brainwave	Frequency Range	Associated Brain Lobes	Functions
Alpha	8-12 Hz	Occipital, Parietal	Relaxation, calmness, wakeful rest, meditation
Beta	13-30 Hz	Frontal, Central (Motor Cortex), Parietal	Active thinking, problem-solving, focus, alertness
Gamma	30-100 Hz	Frontal, Parietal, Temporal	High-level cognitive functions, information processing, learning, memory
Theta	4-8 Hz	Temporal, Frontal	Deep relaxation, light sleep, meditation, creativity, emotional connection
Delta	0.5-4 Hz	Frontal (also present in other regions during deep sleep)	Deep sleep, restorative processes, healing

Figure 23 Types Brain wave frequency

Different brain waves—alpha, beta, and gamma—are active across various brain lobes and play distinct roles in cognitive and sensory processes. Here is a summary of their functions in each of the four main brain lobes:

1. **Frontal Lobe**:
    - **Alpha Waves**- Typically present during relaxed, wakeful states, but are less prominent when the brain is actively engaged in tasks.
    - **Beta Waves**- Strongly associated with active thinking, problem-solving, and decision-making. Beta activity increases in the frontal lobe during tasks that require focus and cognitive engagement.
    - **Gamma Waves**- Linked to high-level cognitive functions, such as attention and complex problem-solving. The frontal lobe shows heightened gamma activity during higher-order thinking and working memory tasks.
2. **Parietal Lobe**:
    - **Alpha Waves**- Commonly observed in relaxed states, particularly with eyes closed, reflecting the inhibition of unnecessary sensory processing.
    - **Beta Waves**- Active during sensory processing and motor control. The parietal lobe exhibits increased beta activity during tasks that involve spatial awareness and sensory integration.

- **Gamma Waves**- Play a key role in integrating sensory information and spatial processing. Gamma activity in the parietal lobe is associated with attention to sensory stimuli and the perception of spatial relationships.

3. **Temporal Lobe**:
    - **Alpha Waves**- Less prominent compared to other regions, as the temporal lobe is primarily involved in processing auditory information.
    - **Beta Waves**- Present during auditory processing and language tasks, with beta activity linked to understanding and processing speech and sounds.
    - **Gamma Waves**- Essential for advanced auditory processing and the integration of auditory and language-related information. Increased gamma activity in the temporal lobe is connected to complex auditory processing and memory retrieval.
4. **Occipital Lobe**:
    - **Alpha Waves**- Prominent in the occipital lobe, especially when the eyes are closed and visual processing is minimal, indicating a relaxed, alert state.
    - **Beta Waves**- Less common but can appear during active visual tasks or cognitive processing of visual information.
    - **Gamma Waves**- Vital for visual processing, including the perception of visual stimuli and the integration of visual details. Gamma activity in the occipital lobe is associated with processing complex visual information.

Each brain wave type contributes to different cognitive and sensory processes, with their presence and intensity varying across brain regions and depending on the specific tasks being performed.

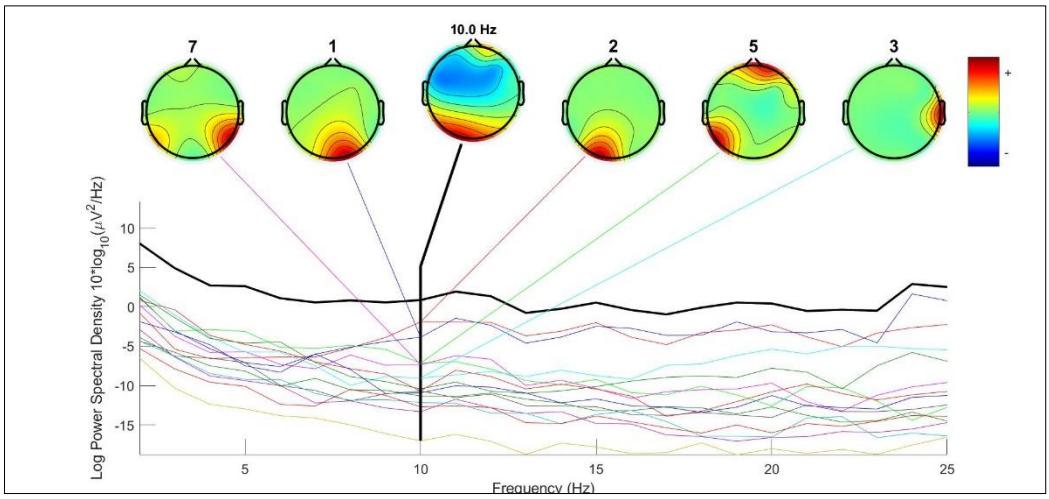

Figure 24 PSD curve at 3000K

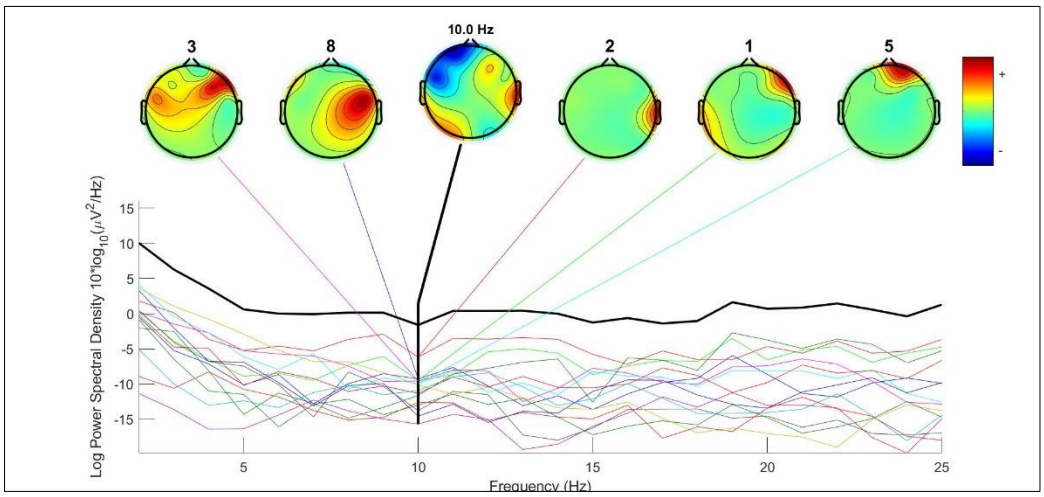

Figure 25 PSD curve at 3000K (VR)

Analysis- From the power spectral density curve, it is evident from the peak that alpha wave active here for both cases.

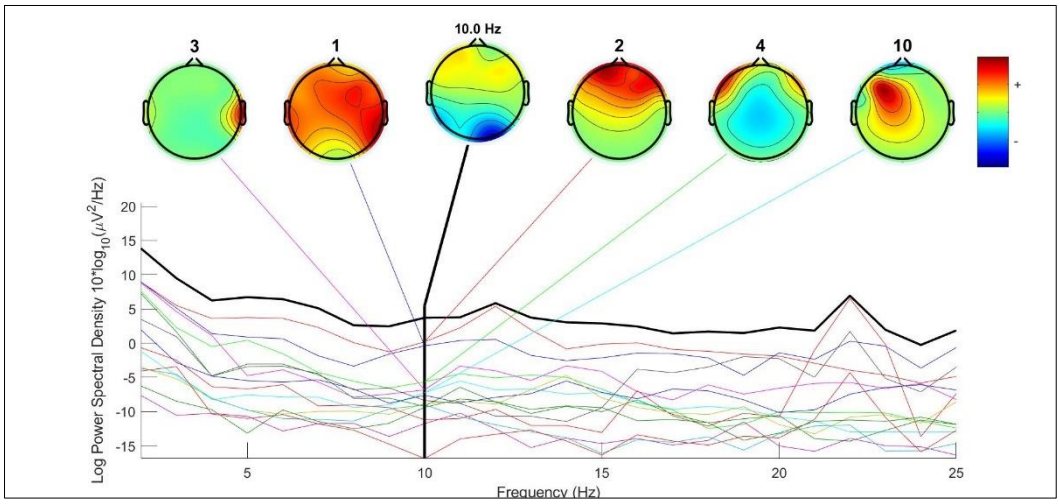

Figure 26 PSD curve at 4000K (VR)

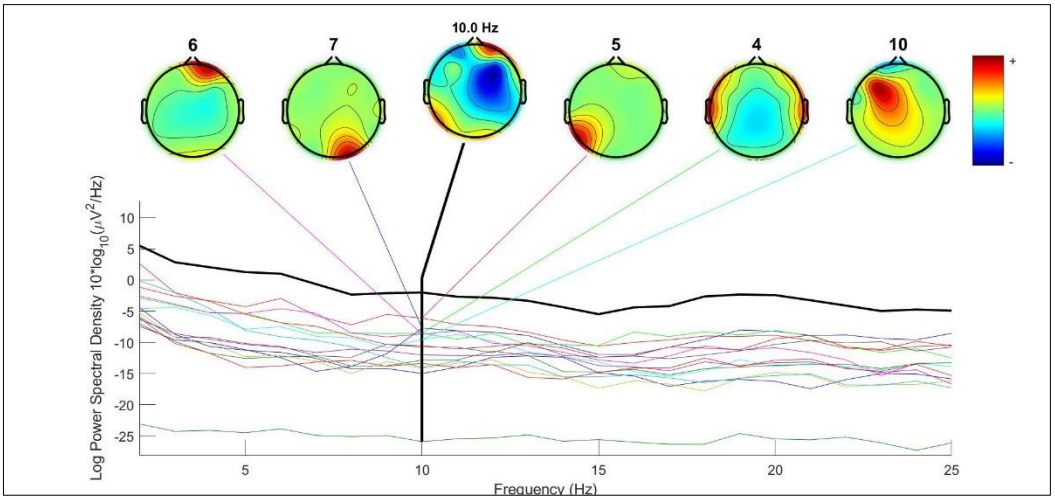

Figure 27 PSD curve at 4000K

Analysis- Here peak at both 10-15hz and 20-25hz observed both alpha and beta wave is active here for both cases.

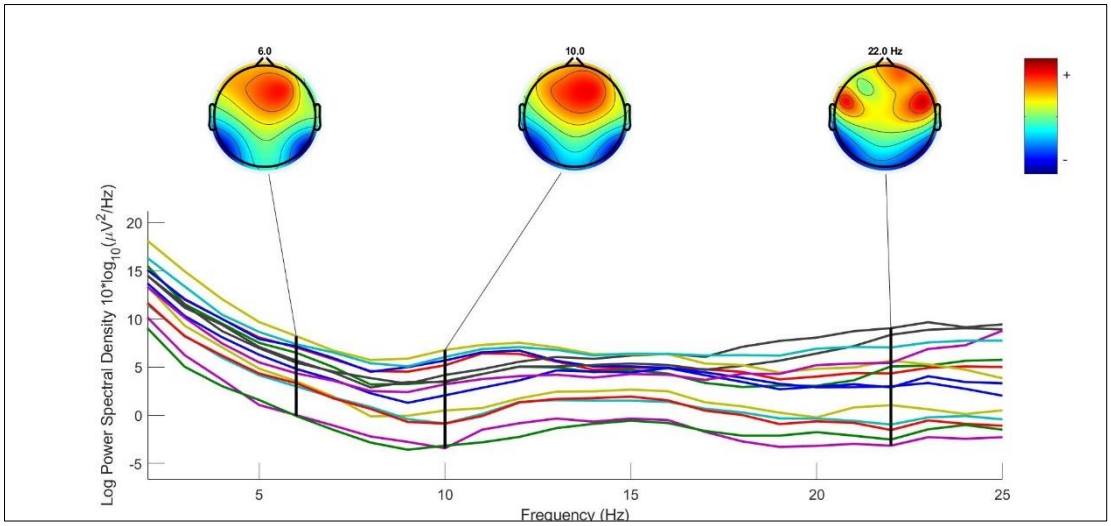

Figure 28 PSD curve at 5000K

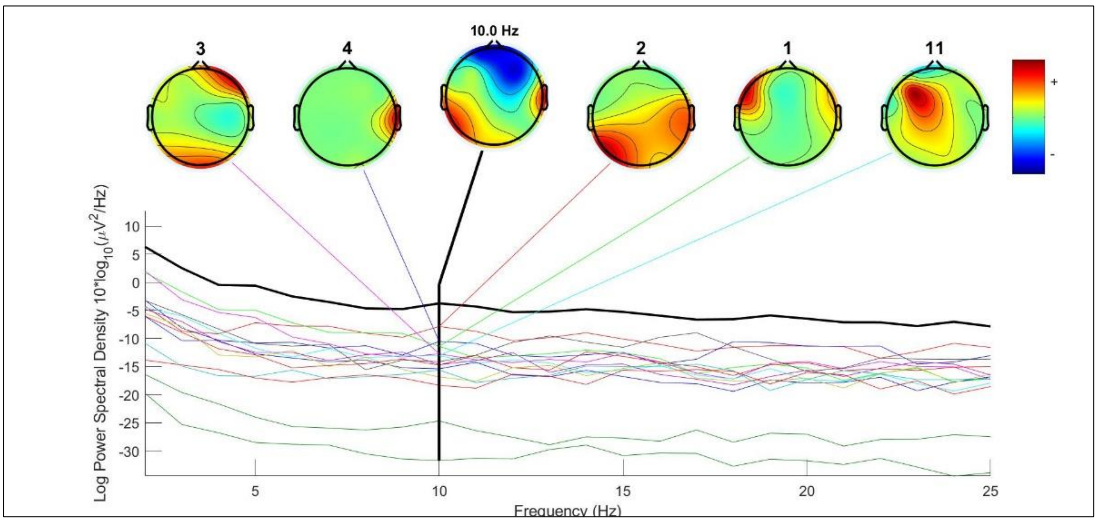

Figure 29 PSD curve at 5000K (VR)

Analysis- Here peak at both 10-15hz and 20-25hz observed. both alpha and beta wave is active here for both cases. Concentration and brain engagement also improved here.

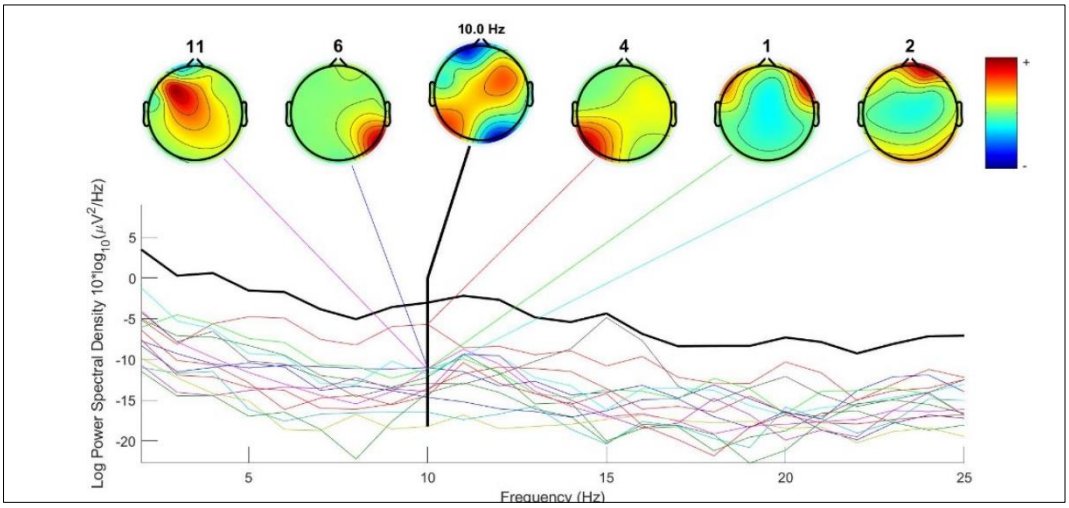

Figure 30 PSD curve at 6000K

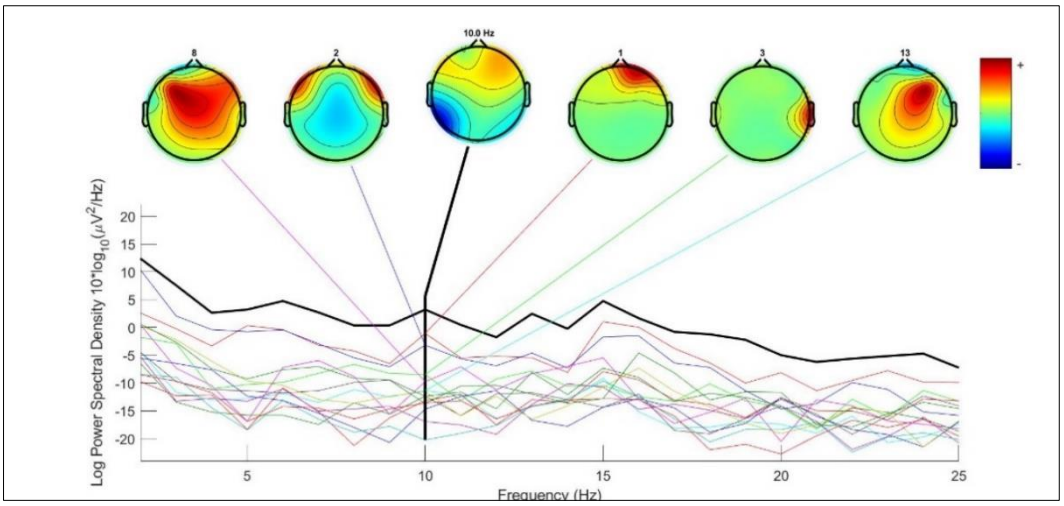

Figure 31 PSD curve at 6000K (VR)

Analysis- Here peak at both 10-15hz and 20-25hz observed. both alpha and beta wave is active here for both cases. Concentration and brain engagement also improved here.

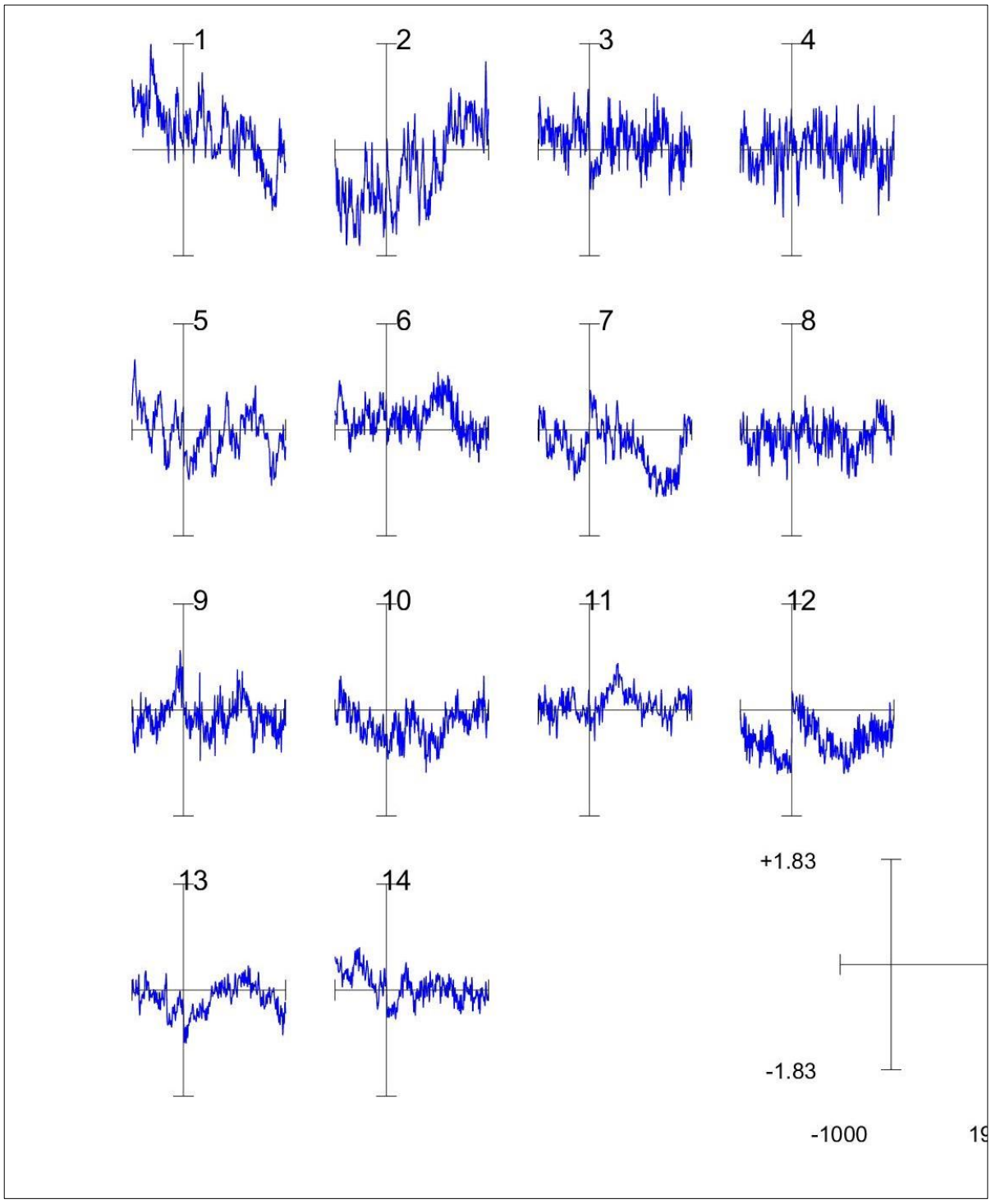

Figure 32 Event related potential (ERP) plot for 6000K

CHAPTER 6

6.1 Introduction to the human-centric street lighting design:

Human-centric street lighting design focuses on optimizing outdoor lighting to enhance the well-being, safety, and comfort of people in urban environments. Unlike traditional street lighting, which primarily aims to illuminate roads and paths for visibility, human-centric lighting considers the biological, psychological, and social effects of light on humans.

The fundamental requirements for road-lighting design, as outlined by the Indian standard (IS1944), primarily emphasize several key principles and classifications which include the level and type of lighting adopted for a street based on traffic importance for both vehicular and pedestrian, type of luminaires, pole arrangement, luminaire distribution, uniformity, illuminance level. However, the safety and comfort of road users significantly decline after dark, especially on roads with inadequately constructed and maintained lighting.

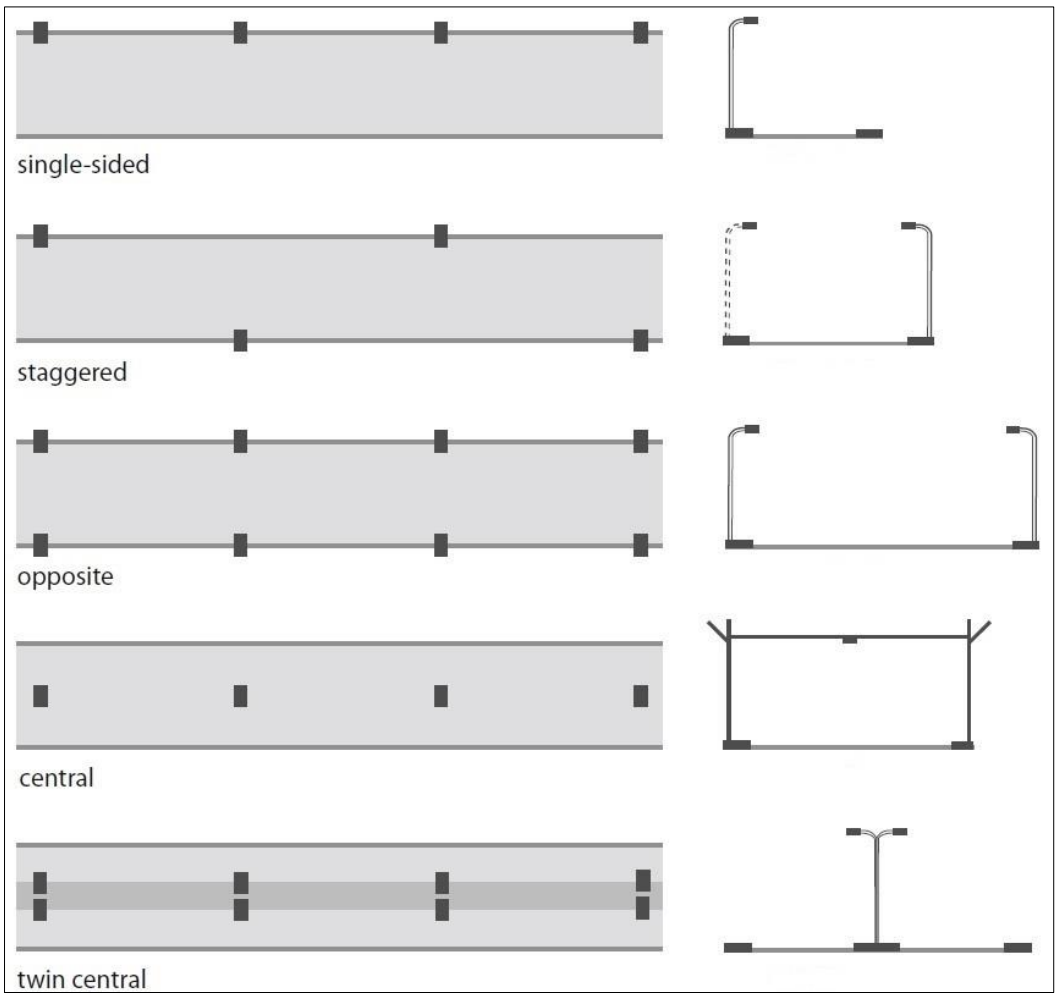

Figure 33 Basic types of street light arrangement

A road lighting configuration refers to the arrangement and design of streetlights to ensure optimal illumination of roadways for safety, visibility, and efficiency.

Key aspects of road lighting arrangements are-

mounting height, Overhang, angle of tilt, spacing between two poles, road width, kerb side.

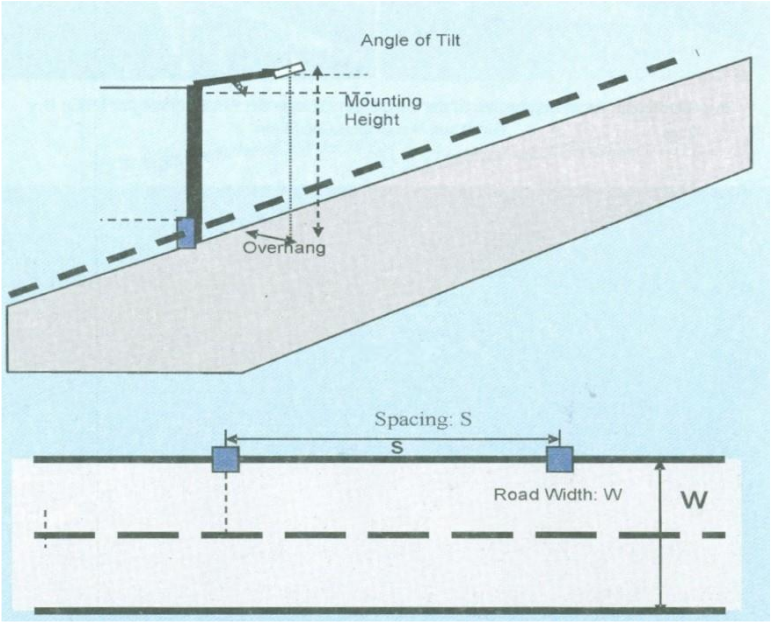

Figure 34 A basic street light configuration

Driving necessitates continuous decision-making based on sensory information. The primary goal of lighting for motorized traffic is to improve the motorist's visual performance, visual comfort, and alertness. A crucial visual task for pedestrians is identifying obstacles. Sufficient obstacle detection in street lighting is a necessary preventative measure against trip hazards and collisions. (W. van Bommel, *Road Lighting*)

Hence design criteria which should be taken into considerations are-

a) **Visibility:** Ensuring clear visibility of the road and its surroundings.

b) **Visual Guidance:** Providing clear identification of road shapes, including bends, curves, and changes in road widths.

c) **Obstacle Identification:** Enabling the clear detection of obstacles.

d) **Visual Comfort:** Maintaining the driver's comfort by considering the entire visual field, which includes the carriageway, surrounding areas, road signs, the sky, and luminaires.

e) **Uniform Lighting:** Ensuring the street lighting appears continuous and uniform. In continuous road lighting design three different criteria are applied which are illuminance criteria, luminance criteria and Small Target visibility criteria.

In road lighting design few aspects are taken into considerations which are-

a) **Energy Efficiency:** Achieved through the selection of efficient lamp technologies and smart design practices.

b) **Capital Cost Savings:** Through proper spacing and placement of lighting fixtures.

c) **Maintenance Cost Reduction:** By using long-lasting lamps and optimizing their spacing.

d) **Reduced Glare and Enhanced Visibility:** Ensured by carefully selecting luminaires and lamps.

e) **Increased Security:** By choosing efficient systems and incorporating thoughtful design, making areas feel safer and more secure.

f) **Economic Development:** Lighting contributes to the perception of economic growth within communities.

g) **Improved Safety:** Enhancing the safety of motorists, cyclists, and pedestrians, along with better traffic guidance and creating a more pleasant environment.

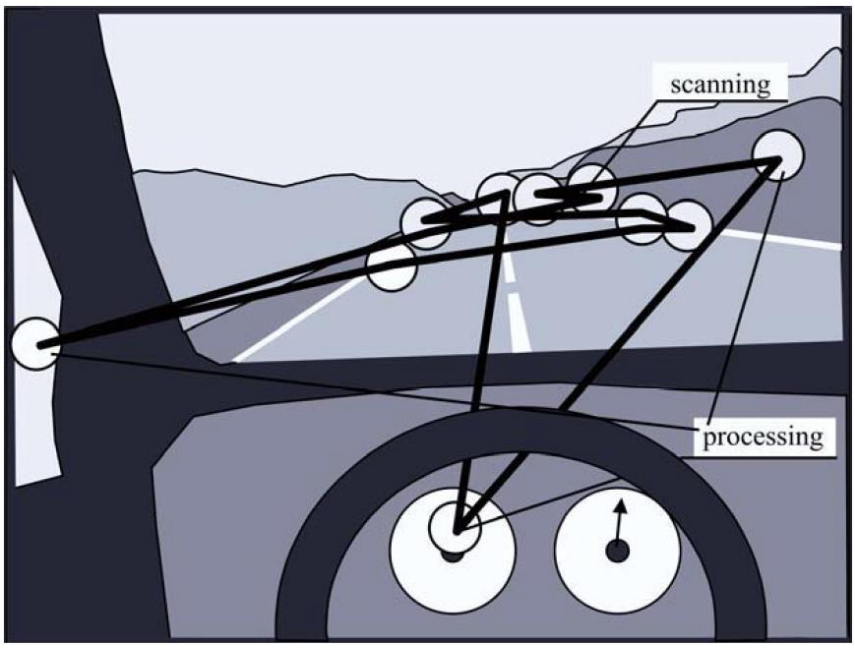

Figure35 Glance behaviour during driving

6.2 Introduction to the VR based experimentation in connection with human-centric street lighting design:

Virtual reality (VR) facilitates spatial presence by providing users with a feeling of being psychologically present while physically being present elsewhere. Virtual Reality (VR) is a powerful tool for experimenting with and designing human-centric street lighting systems. By simulating real-world environments, VR allows researchers and designers to evaluate the impact of different lighting scenarios on human perception, comfort, and safety without the need for physical installations. In the context of human-centric street lighting, VR-based experimentation allows for the controlled examination of numerous parameters such as visibility, glare, uniformity, and visual comfort etc. Participants can explore virtual streetscapes and test various lighting designs and setups. This method enables the evaluation of how lighting effects pedestrian and driver behaviour, obstacle identification, and overall sense of safety. Furthermore, VR experimentation helps to integrate human-centric principles by simulating dynamic lighting circumstances that change depending on the time of day, weather, and user presence. This aids in the refinement of designs that not only meet technical specifications but also improve human well-being and pleasure. Using VR, designers can make informed judgements and optimise lighting. For studying pedestrian and driver behaviour the effect of CCT, small target visibility, reaction time to identify objects, driving fatigue, contrast, visibility level etc could be understood in a more realistic and economical way through VR as road lighting addresses different types visual tasks [W Adrian].

Task performance influenced by lighting conditions are through three pathways which are the visual system, the circadian timing system, and through changes in mood and motivation. In order to study the behavioural and neurocognitive performance under different street lighting conditions one of them being varying CCT given a visual task to be performed, human responses could be obtained by studying brain activity with EEG, electrodermal activity with GSR, reaction time and to feel the sense of realism, VR plays a crucial role here. Lighting plays a direct and indirect role in driving. At night time both rod and cones contribute and participate in the visual performance as well as in the visual periphery of the night time low light level applications [CHI 2020].

Driving involves three simultaneous tasks:

1. **Positional Level**: Routine actions like steering and speed adjustments to stay within the road.
2. **Situational Level**: Adjusting speed or direction in response to changes in the road or environment.
3. **Navigational Level**: Selecting and following the route from start to destination.

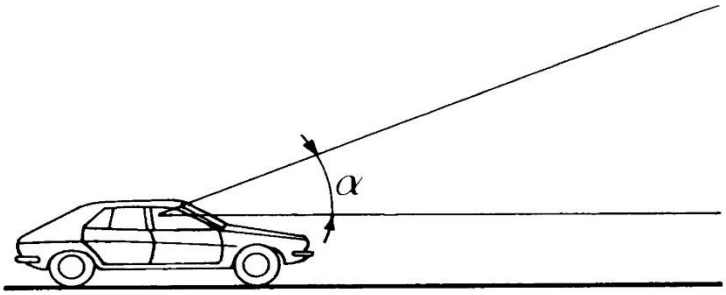

Figure 36 An illustration of viewing angle during driving

Peripheral vision, though not as sharp as foveal vision, plays a crucial role in observation and reading [Rosenholtz, R. (2016)]. While the fovea provides the highest visual acuity, peripheral vision covers everything visible outside the foveal focus [Frey, N. W. (1932)] Visual acuity, resolution, and colour perception decline the further an object is from the point of focus. Despite being less distinct, peripheral vision is essential for detecting motion, which enhances our ability to perceive objects [Solso, R. L. (1996)]. At an arm's length, peripheral vision can only resolve a few tenths of points per inch, compared to the fovea's ability to discern several thousand points. [Johnson, J. (2010)]

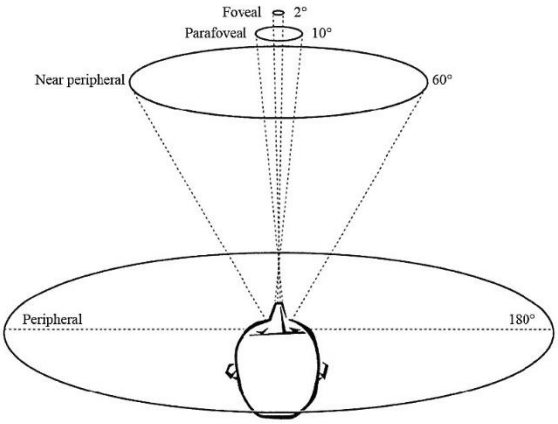

Figure 37 An illustration of foveal, parafoveal, near peripheral and peripheral vision

CHAPTER 7

7.1 DIALux Experimental Design:

7.1.1 Methodology:

DIALux is a lighting design software in which indoor, outdoor street light, daylight, emergency lighting designs are simulated.

Designing a human-centric street lighting system with DIALux is essential for several reasons when setting up a virtual reality (VR) simulation such as -

- **Accurate Lighting Design:** DIALux allows precise modelling of real-world lighting conditions, ensuring that the virtual environment closely matches what would be experienced in real life scenario. This accuracy is essential for VR simulations where the lighting affects user perception and interaction.
- **Standards Compliance:** DIALux enables compliance with relevant lighting standards (like IS1944 in your case), ensuring that the design meets safety, visibility, and comfort criteria. This is vital in VR simulations where realistic and human-centric lighting conditions are necessary for a true-to-life experience.
- **Detailed Photometric Analysis:** DIALux provides detailed photometric data (like illuminance, uniformity, and glare) that can be directly applied in the VR simulation. This ensures that the lighting behaves realistically, affecting how users perceive and navigate the virtual space.
- **Customization and Flexibility:** DIALux offers extensive customization options, such as selecting different luminaires, adjusting pole heights, and configuring light distribution. These details are important for creating specific scenarios in VR simulations, allowing for testing under various conditions.
- **Enhanced User Experience:** A well-designed lighting setup enhances the VR experience by improving visual comfort and realism. Human-centric lighting, which considers factors like colour temperature and light distribution, is critical in VR environments to simulate the desired ambiance and ensure user comfort.
- **Foundation for VR Integration:** By creating a detailed and accurate lighting design in DIALux, you establish a solid foundation that can be imported or replicated in the VR environment. This integration ensures consistency between the design phase and the simulation, making the VR experience more reliable and effective for testing or demonstration purposes.

In summary, DIALux is utilized to develop an accurate, standards-compliant lighting design that serves as the foundation for creating realistic and effective human-centric street lighting simulations in VR.

To create a human-centric street lighting design in DIALux, the following steps were followed:

1) Road Surface and Illuminance Class-

- A 2-lane tarmac road surface was selected, classified under IS1944 standards.
- The A1 illuminance class was chosen for this design.

2) Luminaire Selection-

- A 70-watt, 8800-lumen cool white LED luminaire from Philips was selected.
- This luminaire was imported into the DIALux street lighting project using the luminaire finder.

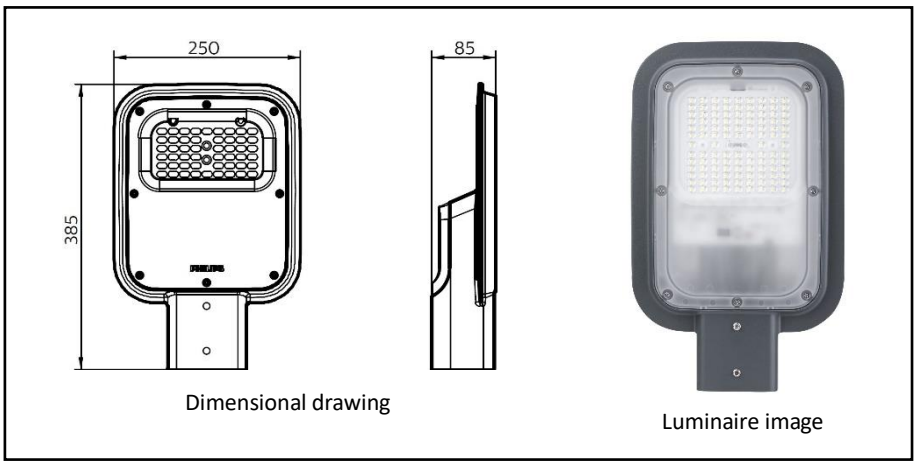

Figure 38 Philips BRP130 LED88

3) Street Light Arrangement-

- A staggered street light arrangement (referred to in DIALux as "double row with offset") was chosen.

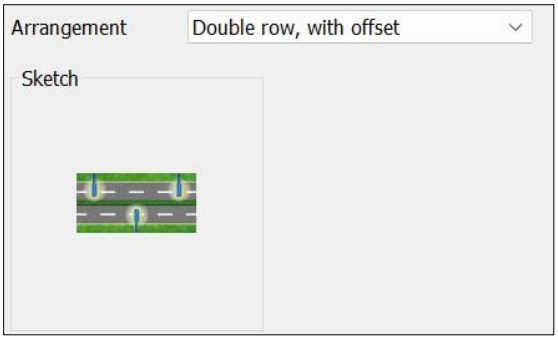

Figure 39 Street light Arrangement

4) Pole Arrangement-

- The poles were arranged with a mounting height of 8 meters.
- The spacing between consecutive poles was set to 30 meters, calculated according to IS1944 to meet design requirements.

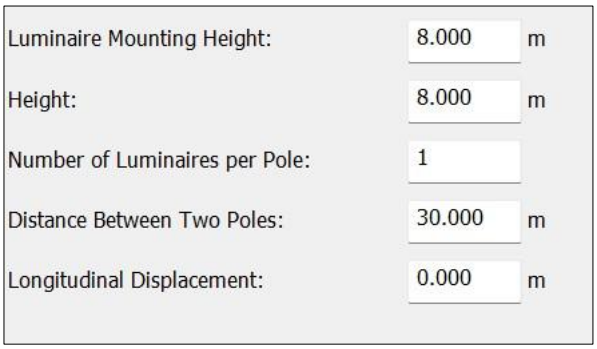

Figure 40 Pole arrangement

5) Additional Specifications-

- The overhang of the luminaire was set at 0.5 meters.
- The distance of the pole from the roadway was 1 meter.
- The tilt angle was set to 0 degrees.
- The boom length was set to 1.5 meters.

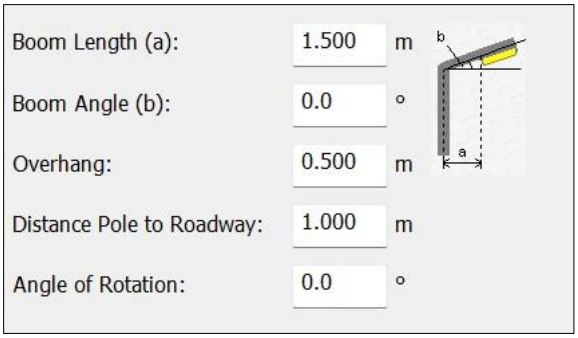

Figure 41 Additional pole arrangements

The above configuration ensures that the street lighting design aligns with the required standards and provides effective illumination for the roadway. After the design requirements and criteria have been met according to the standards, this street lighting design is now ready for implementation in a VR simulation, as discussed in the following section.

7.1.2 DIALux report:

Street 1 / Valuation Field Roadway 1 / Value Chart (E)

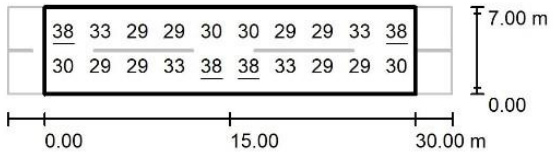

Values in Lux, Scale 1 : 500

Not all calculated values could be displayed.

Grid: 10 x 5 Points

E_{av} [lx]	E_{min} [lx]	E_{max} [lx]	u0	E_{min} / E_{max}
31	24	38	0.789	0.641

Figure 42 Value chart 1

Street 1 / Valuation Field Roadway 1 / Observer 1 / Value Chart (L)

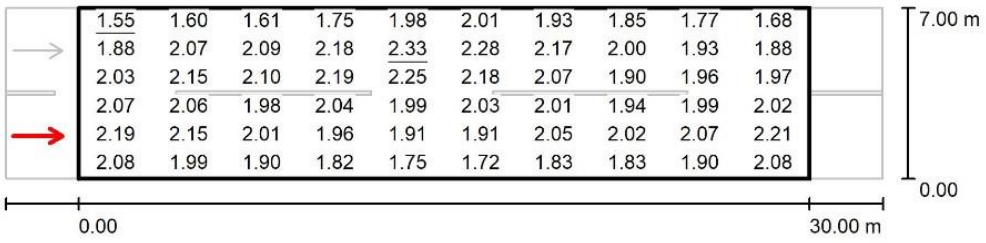

Values in Candela/m², Scale 1 : 258

Grid: 10 x 6 Points
Observer Position: (-60.000 m, 1.750 m, 1.500 m)
tarmac: R3, q0: 0.070

	L_{av} [cd/m²]	U0	UI	TI [%]
Calculated values:	1.98	0.78	0.86	6
Required values according to class ME4a:	≥ 0.75	≥ 0.40	≥ 0.60	≤ 15
Fulfilled/Not fulfilled:	✓	✓	✓	✓

Figure 43 Value chart 2

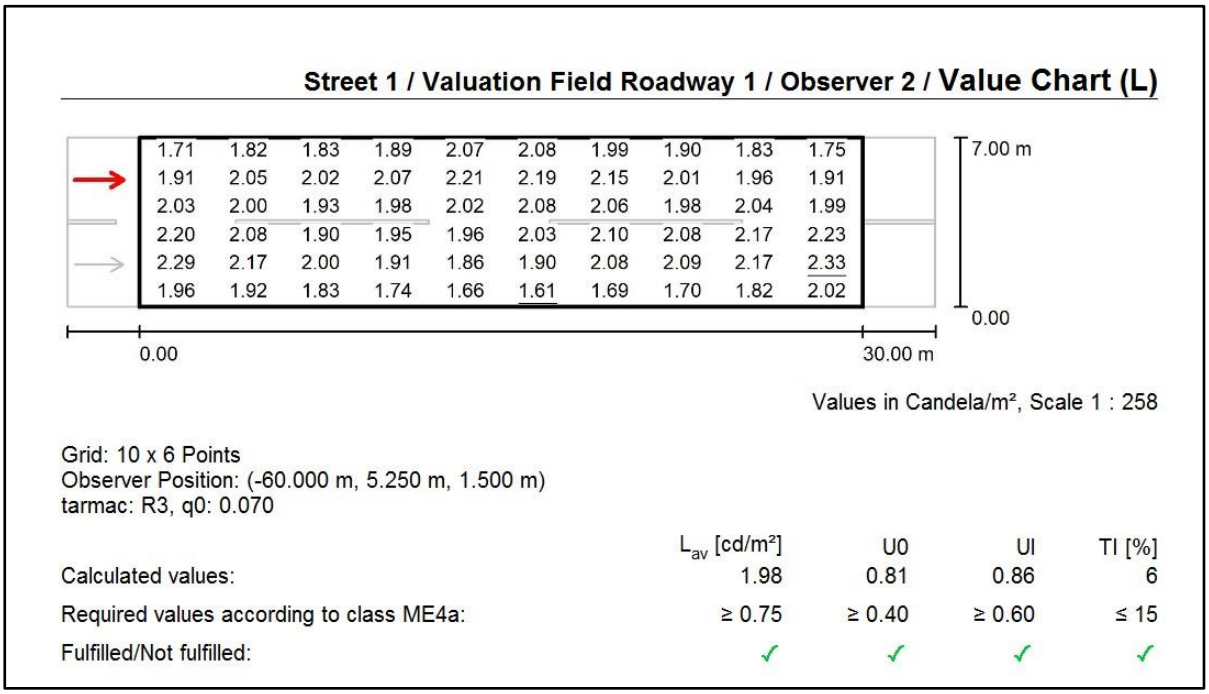

Figure 44 Value chart 3

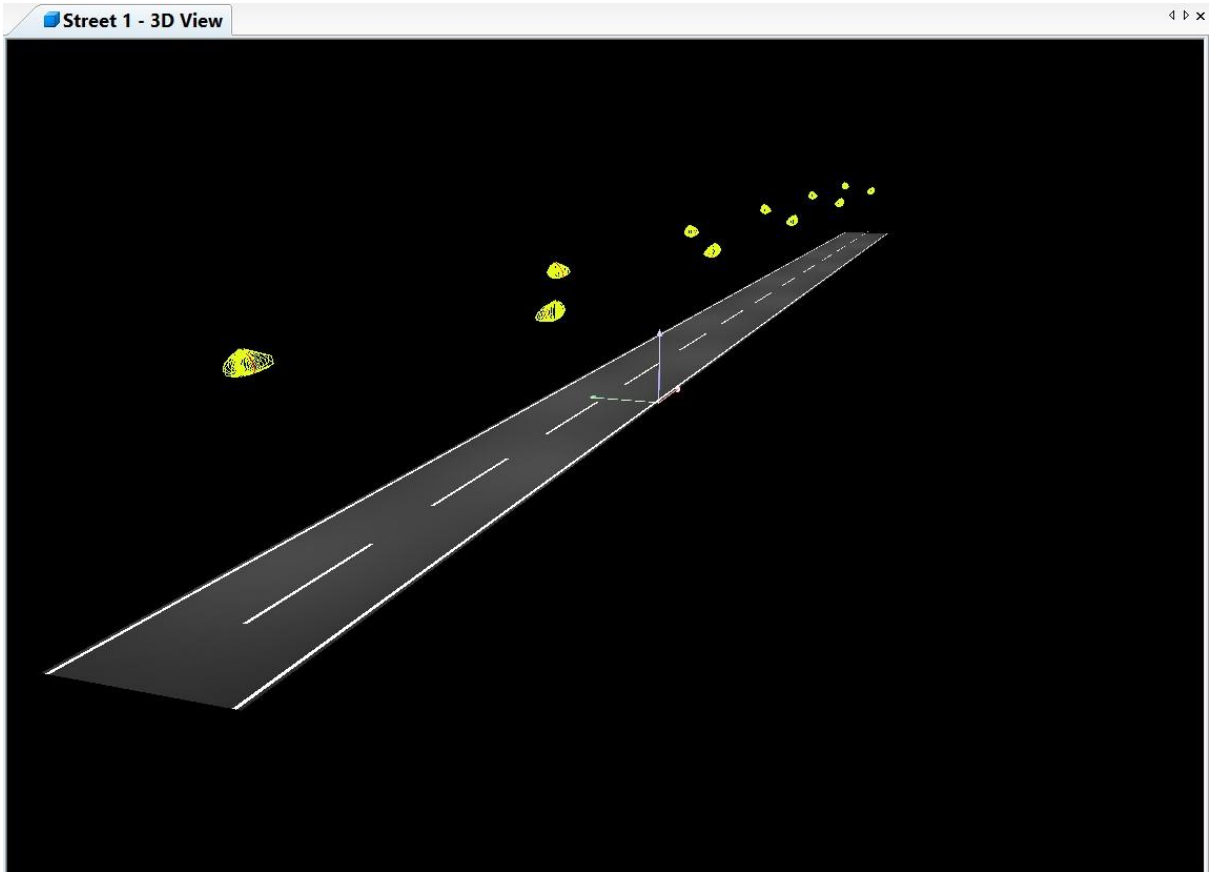

Figure 45 3D view of street lighting design in DIALux

7.2 UNITY Experimental Design:

In this experimental setup, the Unity game engine's High-Definition Render Pipeline (HDRP) version was utilized for its advanced real-time 3D rendering and support for IES files containing photometric data for luminaires. This study aims to assess how CCT influences visual cognition, reaction time, peripheral vision, and physiological responses (such as brain activity and electrodermal response) in a simulated driving environment using virtual reality. By analysing these factors, the experiment seeks to understand the optimal lighting conditions for enhancing driver safety and performance in human-centric street lighting systems.

7.2.1 Simulation Design:

- **3D Asset Preparation and Customization-** All 3D assets were sourced from the Unity Asset Store and customized accordingly.
- **Scaling-** In Unity, a single unit corresponds to one cubic meter in real life, allowing the simulation modelling to be accurately aligned with real-world design parameters.
- **Pole Design-** The poles were modelled to align with the specifications from the DIALux design, featuring a spacing of 30 meters between poles and a mounting height of 8 meters.
- **Photometric Data-** The project used an IES file to provide photometric information, including the staggered pole arrangement, as outlined in the DIALux design. This IES file was imported and set as the IES profile in the Unity project.
- **Luminous Distribution-** A cone pattern was selected for the luminaire's light distribution, with the inner and outer angles determined by the pole height and spacing. In this setup, the inner angle is 75 degrees, and the outer angle is 150 degrees.
- **Vehicle and Obstacle Modelling-** A sedan car model was imported from Unity asset store for the driving simulation, and 30cm x 30cm cubes were created to represent obstacles. These cubes were coloured black, white, and grey.
- **Driving simulation setup-** The simulation involved a 6-minute driving session, with each CCT (3000K, 4500K, and 6000K) lasting 2 minutes. Participants drove a 3D-modeled sedan, and to enhance realism, a first-person camera was positioned at 1 meter to simulate the driver's eye level since drivers viewing angle is 2 degrees. The simulation was designed to mimic a real-world driving scenario, with a first-person

camera view set at eye level to enhance realism. The experiment recorded the number of objects identified, the visibility distance (fixed at 50 meters based on a 1-meter eye height and 2-degree vision), stop time, sight time, and stop distance, which were tracked along the z-axis as the car moved. The simulation was coded in C# using the Unity-supported Microsoft Visual Studio Code editor.

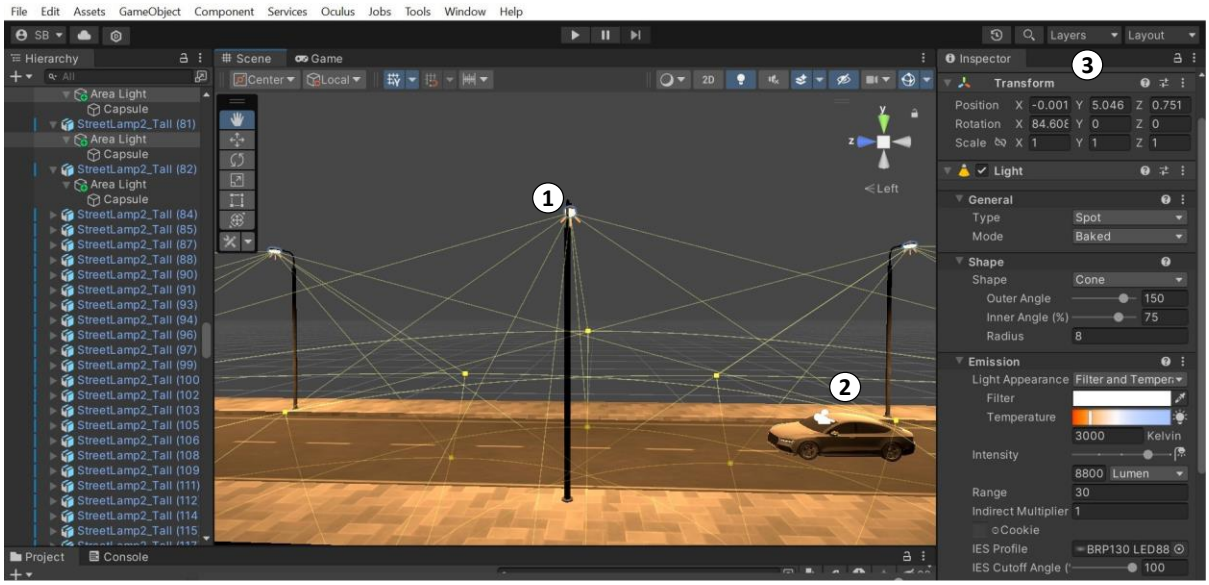

Figure 46 Simulation design in Unity 1) Poles with photometric parameters; 2) Sedan car model for driving simulation in Unity; 3) Design parameters section

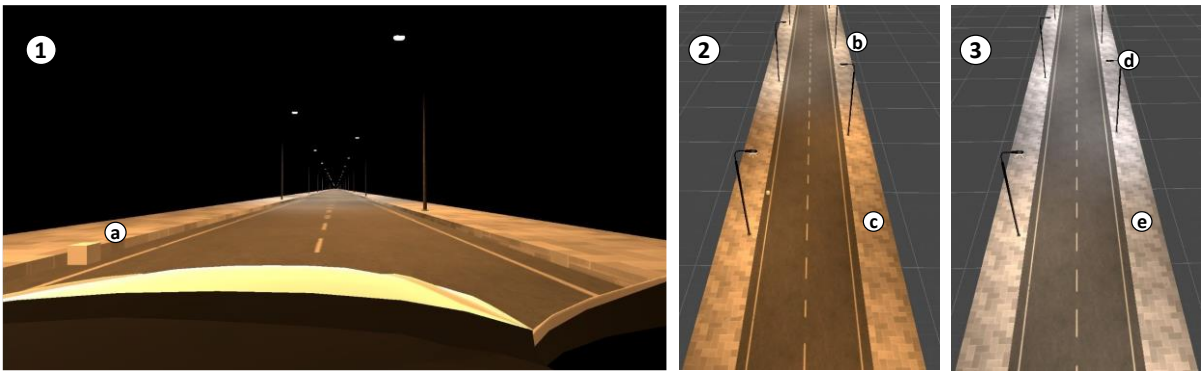

Figure 47 Simulation in action inside Unity
1) Simulation driving scene with first person camera view; a) Object;
3) CCT change from 3000K (c) to 4500K(b)
3) CCT change from 4500K (e) to 6000K(e)

7.2.2 Experimental setup and procedure:

7.2.2.1 *Participants*- Eight participants (n=8), all postgraduate students from Jadavpur University's Electrical Engineering department with normal or corrected to normal vision, participated in the study. They were fully briefed on the task and gave their consent before the experiment. All the participants were university postgraduate students, with ages ranging from 24 to 27 years. The study included 7 male participants and 1 female participant, with an average age of 25.5 years.

7.2.2.2 *Simulation experiment setup*- The experiment took place in the illumination engineering laboratory of the Electrical Engineering Department. The setup included a Meta Quest 2 VR headset, a 14-channel EEG device from EMOTIV, a lab-built GSR device, and two laptops, one for running the simulation and the other for recording EEG data. To begin, each participant was fitted with the Meta Quest 2 headset, ensuring it was comfortable. Prior to this, the 14-channel EMOTIV EEG device had been fully charged, and the felt pads were soaked in a saline gel solution as per the manual's instructions and according to 10-20 system the EEG electrodes were placed onto the scalp of participants. The GSR electrodes were attached to the participant's left hand, specifically on the index and middle fingers. The EEG device was then connected to a laptop via Bluetooth, where the EMOTIV Pro software was pre-installed. Following this, the Meta Quest 2 was connected to the laptop using an Oculus Link cable. EEG recording began with a 2-minute baseline data collection—1 minute with the participant's eyes closed and 1 minute with eyes open. The simulated task then commenced, with events marked at the start and end to capture the EEG activity.

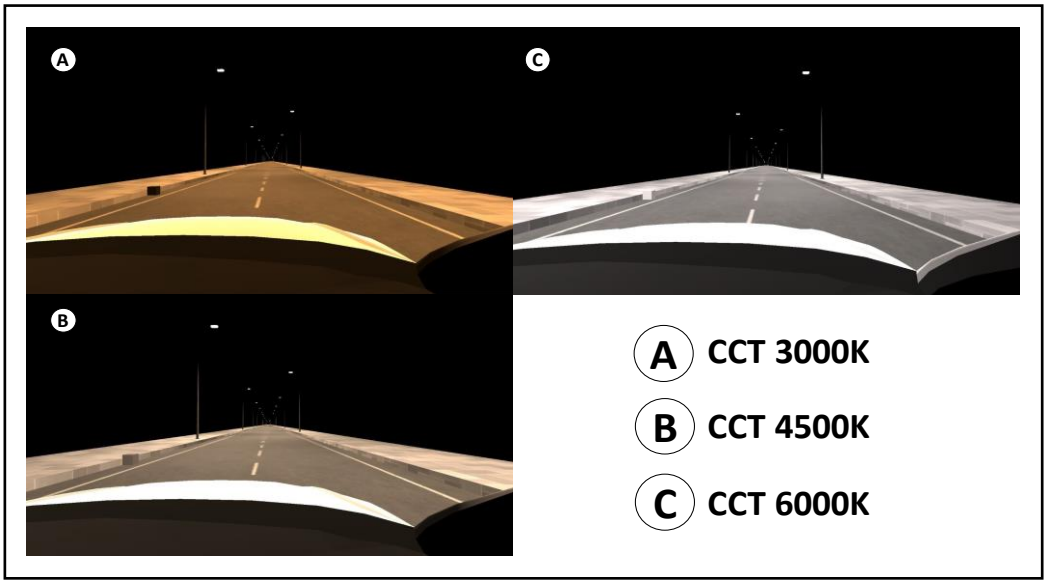

Figure 48 Virtual Reality street-light simulation under three CCTs

7.2.2.3 *Driving simulation task*-

- Participants were placed in a virtual sedan car, which they drove along a continuous stretch of road OF 6 MINUTE DRIVE. The driving simulation was divided into three segments, each lasting 2 minutes, corresponding to different CCTs: 3000K, 4500K, and 6000K.
- The task required participants to identify obstacles (30cm x 30cm cubes) placed along the road. These obstacles were coloured black, white, and grey to assess the impact of different CCTs on visibility and object recognition.
- Participants were instructed to drive, identify obstacles, and respond by braking or pausing when an obstacle was recognized. The interaction was designed to simulate real-world driving conditions and measure the participants' response times and accuracy.

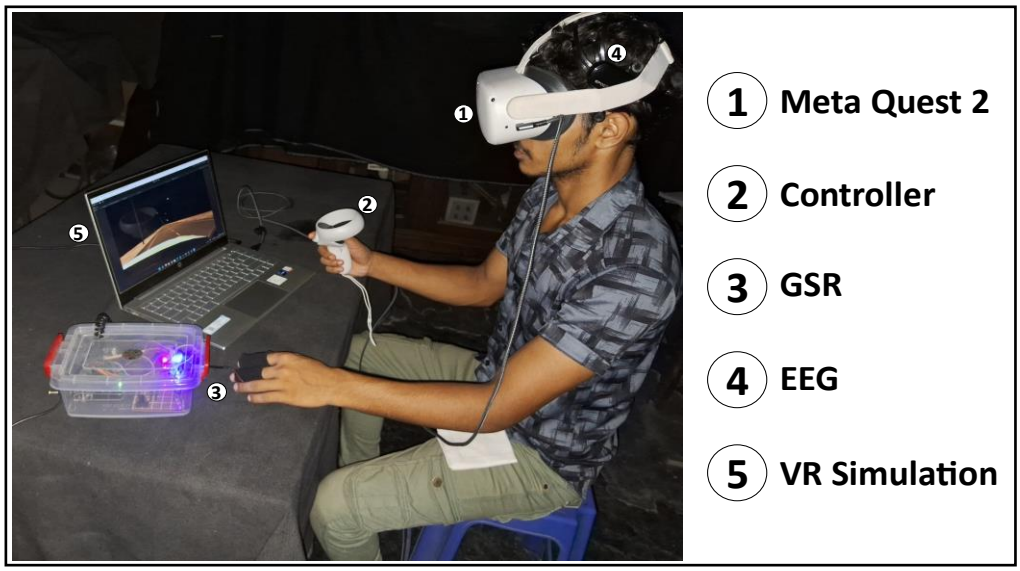

Figure 49 Virtual Reality driving simulation experiment in progress

7.2.2.4 *Data recording*- The virtual reality experiment tracked the number of obstacles identified, the distance at which each obstacle became visible, and additional metrics such as stop time, sight time, and stop distance. It also monitored physiological responses, including brain activity (via EEG) and electrodermal response (via GSR), throughout the task. Two key events were marked in the EEG recordings: one at the start of the task and another at the end. These markers were used to calculate the reaction time of the participants.

7.3 Experimental Workflow:

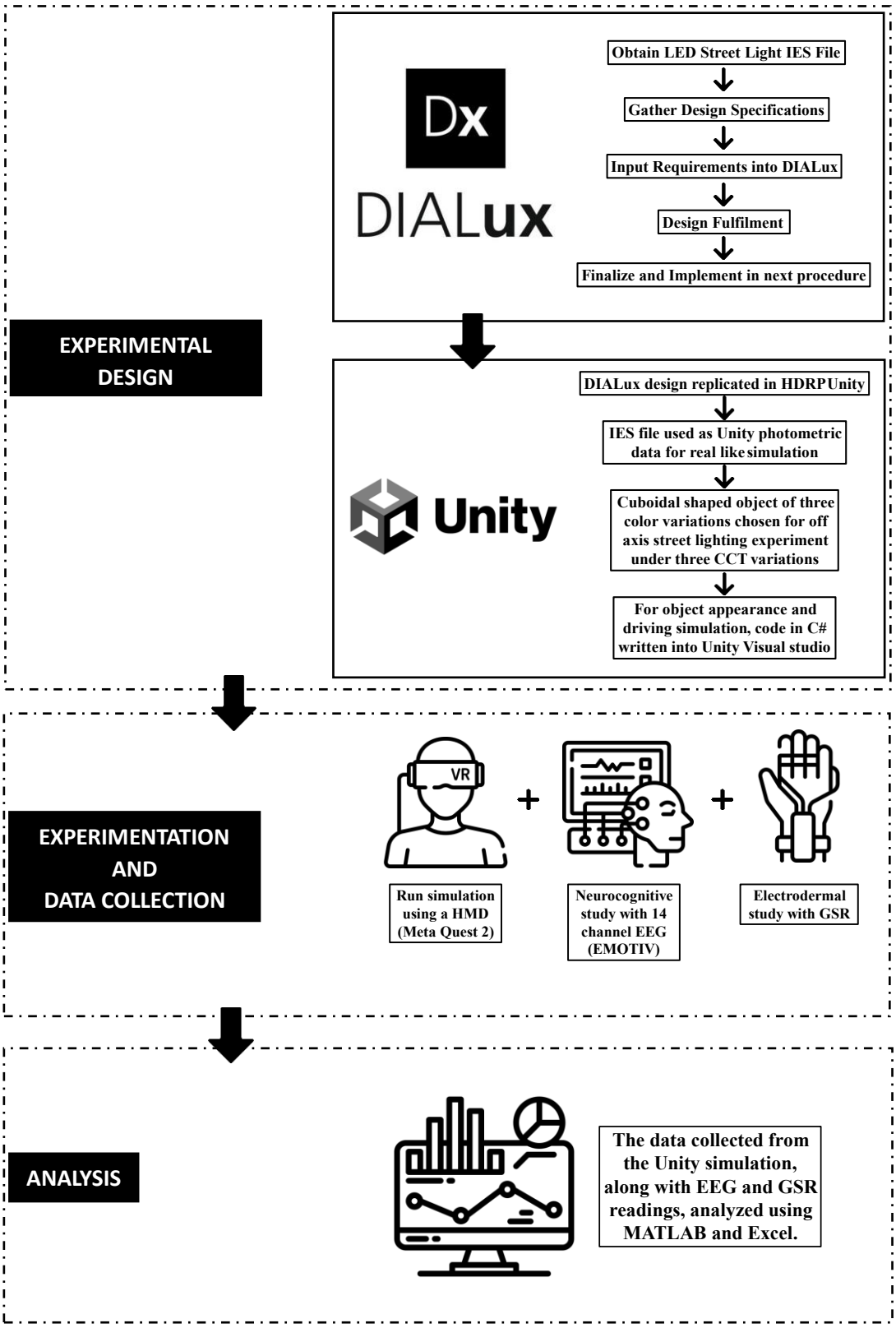

CHAPTER 8

8.1 Result and Analysis:

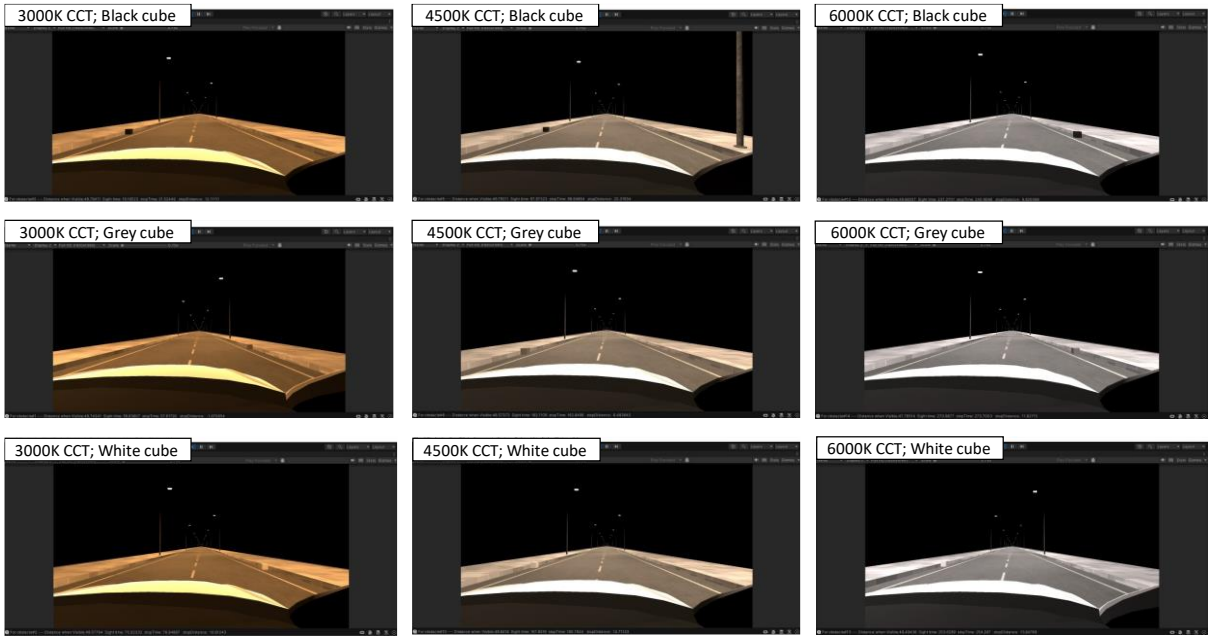

Figure 50 Virtual Reality driving simulation experiment in progress under three different CCTs (3000K, 4500K, 6000K) with three different coloured cubes placed for object detection (Black, Grey, White).

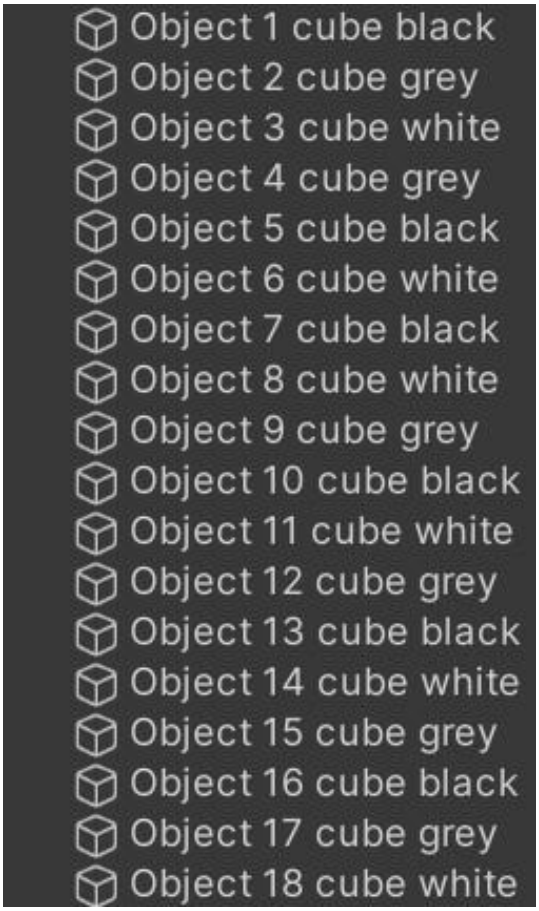

Figure 51 Object appearance order in simulation

```
For obstacle#0 --- Distance when Visible:49.78229  Sight time: 278.6006  stopTime: 279.65   stopDistance:  38.01851
For obstacle#1 --- Distance when Visible:49.99496  Sight time: 299.1682  stopTime: 300.2695   stopDistance:  37.61044
For obstacle#2 --- Distance when Visible:49.88678  Sight time: 319.6707  stopTime: 320.5305   stopDistance:  40.2475
For obstacle#3 --- Distance when Visible:49.78882  Sight time: 339.9016  stopTime: 341.1013   stopDistance:  36.31036
For obstacle#4 --- Distance when Visible:49.84729  Sight time: 360.2399  stopTime: 361.0748   stopDistance:  40.58496
For obstacle#5 --- Distance when Visible:49.70593  Sight time: 380.556  stopTime: 401.3893   stopDistance:  -185.8735
For obstacle#6 --- Distance when Visible:49.95996  Sight time: 400.4233  stopTime: 401.3893   stopDistance:  39.12646
For obstacle#7 --- Distance when Visible:49.98499  Sight time: 420.869  stopTime: 442.1779   stopDistance:  -190.9752
For obstacle#8 --- Distance when Visible:49.78735  Sight time: 440.7743  stopTime: 442.1779   stopDistance:  34.02478
For obstacle#9 --- Distance when Visible:49.91821  Sight time: 461.1107  stopTime: 461.7678   stopDistance:  42.56787
For obstacle#10 --- Distance when Visible:49.92651  Sight time: 481.338  stopTime: 502.0857   stopDistance:  -184.6914
For obstacle#11 --- Distance when Visible:49.96094  Sight time: 501.2233  stopTime: 502.0857   stopDistance:  40.30859
For obstacle#12 --- Distance when Visible:49.94043  Sight time: 521.5728  stopTime: 522.4244   stopDistance:  40.42993
For obstacle#13 --- Distance when Visible:49.85376  Sight time: 542.0789  stopTime: 563.7507   stopDistance:  -195.199
For obstacle#14 --- Distance when Visible:49.94751  Sight time: 561.959  stopTime: 563.7507   stopDistance:  29.80103
For obstacle#15 --- Distance when Visible:49.96777  Sight time: 582.1987  stopTime: 583.2153   stopDistance:  38.56958
For obstacle#16 --- Distance when Visible:49.88989  Sight time: 602.0806  stopTime: 602.9646   stopDistance:  40.04736
For obstacle#17 --- Distance when Visible:49.97461  Sight time: 622.7125  stopTime: 625.0261   stopDistance:  23.98218
```

```
For obstacle#0 --- Distance when Visible:49.81233  Sight time: 202.3763  stopTime: 286.2499   stopDistance:  -899.0037
For obstacle#1 --- Distance when Visible:49.88782  Sight time: 222.2569  stopTime: 286.2499   stopDistance:  -674.0037
For obstacle#2 --- Distance when Visible:49.7522  Sight time: 242.1564  stopTime: 286.2499   stopDistance:  -449.0037
For obstacle#3 --- Distance when Visible:49.99451  Sight time: 262.0217  stopTime: 286.2499   stopDistance:  -224.0037
For obstacle#4 --- Distance when Visible:49.95349  Sight time: 281.9134  stopTime: 286.2499   stopDistance:  0.9963379
For obstacle#5 --- Distance when Visible:49.88281  Sight time: 305.7815  stopTime: 309.761   stopDistance:  5.005493
For obstacle#6 --- Distance when Visible:49.78137  Sight time: 333.0295  stopTime: 337.1382   stopDistance:  3.37085
For obstacle#7 --- Distance when Visible:49.91785  Sight time: 355.8789  stopTime: 399.7899   stopDistance:  -446.7712
For obstacle#8 --- Distance when Visible:49.91235  Sight time: 375.7672  stopTime: 399.7899   stopDistance:  -221.7712
For obstacle#9 --- Distance when Visible:49.94629  Sight time: 395.6519  stopTime: 399.7899   stopDistance:  3.22876
For obstacle#10 --- Distance when Visible:49.90479  Sight time: 417.6266  stopTime: 441.4999   stopDistance:  -220.0867
For obstacle#11 --- Distance when Visible:49.93677  Sight time: 437.5105  stopTime: 441.4999   stopDistance:  4.91333
For obstacle#12 --- Distance when Visible:49.76636  Sight time: 460.1347  stopTime: 464.0332   stopDistance:  5.778564
For obstacle#13 --- Distance when Visible:49.82788  Sight time: 481.4309  stopTime: 505.1941   stopDistance:  -218.9155
For obstacle#14 --- Distance when Visible:49.823  Sight time: 501.3177  stopTime: 505.1941   stopDistance:  6.084473
For obstacle#15 --- Distance when Visible:49.93896  Sight time: 522.9058  stopTime: 526.7518   stopDistance:  6.532715
For obstacle#16 --- Distance when Visible:49.77124  Sight time: 543.905  stopTime: 547.5648   stopDistance:  8.447021
For obstacle#17 --- Distance when Visible:49.93359  Sight time: 565.6807  stopTime: 575.196   stopDistance:  -57.61182
```

```
For obstacle#0 --- Distance when Visible:49.96506  Sight time: 54.3418  stopTime: 57.35005   stopDistance:  16.03371
For obstacle#1 --- Distance when Visible:49.79196  Sight time: 83.01206  stopTime: 145.4216   stopDistance:  -656.2103
For obstacle#2 --- Distance when Visible:49.9389  Sight time: 102.8866  stopTime: 145.4216   stopDistance:  -431.2103
For obstacle#3 --- Distance when Visible:49.93848  Sight time: 122.774  stopTime: 145.4216   stopDistance:  -206.2103
For obstacle#4 --- Distance when Visible:49.89624  Sight time: 142.6646  stopTime: 145.4216   stopDistance:  18.78967
For obstacle#5 --- Distance when Visible:49.91418  Sight time: 163.5306  stopTime: 185.3407   stopDistance:  -196.7267
For obstacle#6 --- Distance when Visible:49.89819  Sight time: 183.4189  stopTime: 185.3407   stopDistance:  28.27332
For obstacle#7 --- Distance when Visible:49.84827  Sight time: 204.1574  stopTime: 228.1662   stopDistance:  -221.692
For obstacle#8 --- Distance when Visible:49.84204  Sight time: 224.045  stopTime: 228.1662   stopDistance:  3.307983
For obstacle#9 --- Distance when Visible:49.92163  Sight time: 245.6898  stopTime: 247.8759   stopDistance:  25.29858
For obstacle#10 --- Distance when Visible:49.96899  Sight time: 266.6441  stopTime: 289.5334   stopDistance:  -208.8779
For obstacle#11 --- Distance when Visible:49.9978  Sight time: 286.5314  stopTime: 289.5334   stopDistance:  16.12207
For obstacle#12 --- Distance when Visible:49.95654  Sight time: 307.5603  stopTime: 309.991   stopDistance:  22.6167
For obstacle#13 --- Distance when Visible:49.98608  Sight time: 328.2763  stopTime: 351.1206   stopDistance:  -208.3645
For obstacle#14 --- Distance when Visible:49.88428  Sight time: 348.1723  stopTime: 351.1206   stopDistance:  16.6355
For obstacle#15 --- Distance when Visible:49.98608  Sight time: 368.8314  stopTime: 371.1116   stopDistance:  24.32178
For obstacle#16 --- Distance when Visible:49.74194  Sight time: 389.0362  stopTime: 391.3732   stopDistance:  23.40747
For obstacle#17 --- Distance when Visible:49.97144  Sight time: 410.0559  stopTime: 418.644   stopDistance:  -47.10693
```

```
For obstacle#0 --- Distance when Visible:49.90125  Sight time: 472.8605  stopTime: 476.722   stopDistance:  6.329376
For obstacle#1 --- Distance when Visible:49.91757  Sight time: 493.1829  stopTime: 516.8283   stopDistance:  -217.5108
For obstacle#2 --- Distance when Visible:49.85364  Sight time: 513.0748  stopTime: 516.8283   stopDistance:  7.489197
For obstacle#3 --- Distance when Visible:49.89178  Sight time: 533.4752  stopTime: 537.0913   stopDistance:  9.049194
For obstacle#4 --- Distance when Visible:49.76709  Sight time: 553.8756  stopTime: 557.4927   stopDistance:  8.954956
For obstacle#5 --- Distance when Visible:49.76624  Sight time: 574.1708  stopTime: 577.9716   stopDistance:  6.870728
For obstacle#6 --- Distance when Visible:49.97607  Sight time: 594.4191  stopTime: 598.2351   stopDistance:  6.948853
For obstacle#7 --- Distance when Visible:49.797  Sight time: 614.7136  stopTime: 618.2984   stopDistance:  9.351563
For obstacle#8 --- Distance when Visible:49.96411  Sight time: 635.0529  stopTime: 638.813   stopDistance:  7.556396
For obstacle#9 --- Distance when Visible:49.96167  Sight time: 655.3985  stopTime: 659.0836   stopDistance:  8.368408
For obstacle#10 --- Distance when Visible:49.84863  Sight time: 675.6937  stopTime: 679.2933   stopDistance:  9.263672
For obstacle#11 --- Distance when Visible:49.85986  Sight time: 696.0381  stopTime: 699.8318   stopDistance:  7.042969
For obstacle#12 --- Distance when Visible:49.82373  Sight time: 716.4313  stopTime: 719.9093   stopDistance:  10.53809
For obstacle#13 --- Distance when Visible:49.95728  Sight time: 736.7197  stopTime: 740.3059   stopDistance:  9.523926
For obstacle#14 --- Distance when Visible:49.97339  Sight time: 757.0465  stopTime: 760.4468   stopDistance:  11.61743
For obstacle#15 --- Distance when Visible:49.90894  Sight time: 777.3541  stopTime: 781.189   stopDistance:  6.606934
For obstacle#16 --- Distance when Visible:49.77808  Sight time: 797.1338  stopTime: 800.8259   stopDistance:  8.100586
For obstacle#17 --- Distance when Visible:49.85156  Sight time: 817.908  stopTime: 821.5573   stopDistance:  8.680908
```

Figure 52a Experimental response output from VR simulation

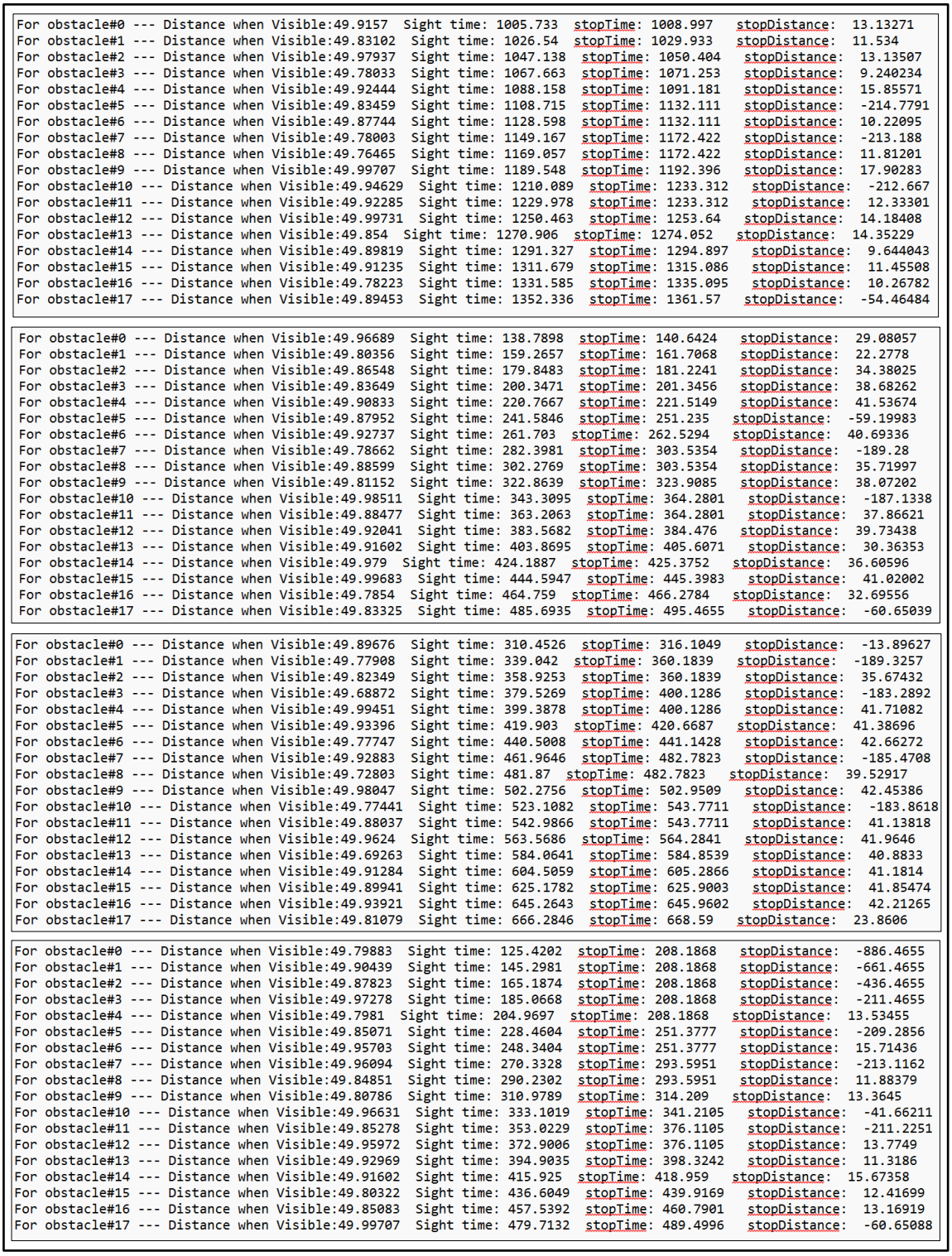

```
For obstacle#0 --- Distance when Visible:49.9157  Sight time: 1005.733  stopTime: 1008.997   stopDistance:  13.13271
For obstacle#1 --- Distance when Visible:49.83102  Sight time: 1026.54  stopTime: 1029.933   stopDistance:  11.534
For obstacle#2 --- Distance when Visible:49.97937  Sight time: 1047.138  stopTime: 1050.404   stopDistance:  13.13507
For obstacle#3 --- Distance when Visible:49.78033  Sight time: 1067.663  stopTime: 1071.253   stopDistance:  9.240234
For obstacle#4 --- Distance when Visible:49.92444  Sight time: 1088.158  stopTime: 1091.181   stopDistance:  15.85571
For obstacle#5 --- Distance when Visible:49.83459  Sight time: 1108.715  stopTime: 1132.111   stopDistance:  -214.7791
For obstacle#6 --- Distance when Visible:49.87744  Sight time: 1128.598  stopTime: 1132.111   stopDistance:  10.22095
For obstacle#7 --- Distance when Visible:49.78003  Sight time: 1149.167  stopTime: 1172.422   stopDistance:  -213.188
For obstacle#8 --- Distance when Visible:49.76465  Sight time: 1169.057  stopTime: 1172.422   stopDistance:  11.81201
For obstacle#9 --- Distance when Visible:49.99707  Sight time: 1189.548  stopTime: 1192.396   stopDistance:  17.90283
For obstacle#10 --- Distance when Visible:49.94629  Sight time: 1210.089  stopTime: 1233.312   stopDistance:  -212.667
For obstacle#11 --- Distance when Visible:49.92285  Sight time: 1229.978  stopTime: 1233.312   stopDistance:  12.33301
For obstacle#12 --- Distance when Visible:49.99731  Sight time: 1250.463  stopTime: 1253.64   stopDistance:  14.18408
For obstacle#13 --- Distance when Visible:49.854  Sight time: 1270.906  stopTime: 1274.052   stopDistance:  14.35229
For obstacle#14 --- Distance when Visible:49.89819  Sight time: 1291.327  stopTime: 1294.897   stopDistance:  9.644043
For obstacle#15 --- Distance when Visible:49.91235  Sight time: 1311.679  stopTime: 1315.086   stopDistance:  11.45508
For obstacle#16 --- Distance when Visible:49.78223  Sight time: 1331.585  stopTime: 1335.095   stopDistance:  10.26782
For obstacle#17 --- Distance when Visible:49.89453  Sight time: 1352.336  stopTime: 1361.57   stopDistance:  -54.46484

For obstacle#0 --- Distance when Visible:49.96689  Sight time: 138.7898  stopTime: 140.6424   stopDistance:  29.08057
For obstacle#1 --- Distance when Visible:49.80356  Sight time: 159.2657  stopTime: 161.7068   stopDistance:  22.2778
For obstacle#2 --- Distance when Visible:49.86548  Sight time: 179.8483  stopTime: 181.2241   stopDistance:  34.38025
For obstacle#3 --- Distance when Visible:49.83649  Sight time: 200.3471  stopTime: 201.3456   stopDistance:  38.68262
For obstacle#4 --- Distance when Visible:49.90833  Sight time: 220.7667  stopTime: 221.5149   stopDistance:  41.53674
For obstacle#5 --- Distance when Visible:49.87952  Sight time: 241.5846  stopTime: 251.235   stopDistance:  -59.19983
For obstacle#6 --- Distance when Visible:49.92737  Sight time: 261.703  stopTime: 262.5294   stopDistance:  40.69336
For obstacle#7 --- Distance when Visible:49.78662  Sight time: 282.3981  stopTime: 303.5354   stopDistance:  -189.28
For obstacle#8 --- Distance when Visible:49.88599  Sight time: 302.2769  stopTime: 303.5354   stopDistance:  35.71997
For obstacle#9 --- Distance when Visible:49.81152  Sight time: 322.8639  stopTime: 323.9085   stopDistance:  38.07202
For obstacle#10 --- Distance when Visible:49.98511  Sight time: 343.3095  stopTime: 364.2801   stopDistance:  -187.1338
For obstacle#11 --- Distance when Visible:49.88477  Sight time: 363.2063  stopTime: 364.2801   stopDistance:  37.86621
For obstacle#12 --- Distance when Visible:49.92041  Sight time: 383.5682  stopTime: 384.476   stopDistance:  39.73438
For obstacle#13 --- Distance when Visible:49.91602  Sight time: 403.8695  stopTime: 405.6071   stopDistance:  30.36353
For obstacle#14 --- Distance when Visible:49.979  Sight time: 424.1887  stopTime: 425.3752   stopDistance:  36.60596
For obstacle#15 --- Distance when Visible:49.99683  Sight time: 444.5947  stopTime: 445.3983   stopDistance:  41.02002
For obstacle#16 --- Distance when Visible:49.7854  Sight time: 464.759  stopTime: 466.2784   stopDistance:  32.69556
For obstacle#17 --- Distance when Visible:49.83325  Sight time: 485.6935  stopTime: 495.4655   stopDistance:  -60.65039

For obstacle#0 --- Distance when Visible:49.89676  Sight time: 310.4526  stopTime: 316.1049   stopDistance:  -13.89627
For obstacle#1 --- Distance when Visible:49.77908  Sight time: 339.042  stopTime: 360.1839   stopDistance:  -189.3257
For obstacle#2 --- Distance when Visible:49.82349  Sight time: 358.9253  stopTime: 360.1839   stopDistance:  35.67432
For obstacle#3 --- Distance when Visible:49.68872  Sight time: 379.5269  stopTime: 400.1286   stopDistance:  -183.2892
For obstacle#4 --- Distance when Visible:49.99451  Sight time: 399.3878  stopTime: 400.1286   stopDistance:  41.71082
For obstacle#5 --- Distance when Visible:49.93396  Sight time: 419.903  stopTime: 420.6687   stopDistance:  41.38696
For obstacle#6 --- Distance when Visible:49.77747  Sight time: 440.5008  stopTime: 441.1428   stopDistance:  42.66272
For obstacle#7 --- Distance when Visible:49.92883  Sight time: 461.9646  stopTime: 482.7823   stopDistance:  -185.4708
For obstacle#8 --- Distance when Visible:49.72803  Sight time: 481.87  stopTime: 482.7823   stopDistance:  39.52917
For obstacle#9 --- Distance when Visible:49.98047  Sight time: 502.2756  stopTime: 502.9509   stopDistance:  42.45386
For obstacle#10 --- Distance when Visible:49.77441  Sight time: 523.1082  stopTime: 543.7711   stopDistance:  -183.8618
For obstacle#11 --- Distance when Visible:49.88037  Sight time: 542.9866  stopTime: 543.7711   stopDistance:  41.13818
For obstacle#12 --- Distance when Visible:49.9624  Sight time: 563.5686  stopTime: 564.2841   stopDistance:  41.9646
For obstacle#13 --- Distance when Visible:49.69263  Sight time: 584.0641  stopTime: 584.8539   stopDistance:  40.8833
For obstacle#14 --- Distance when Visible:49.91284  Sight time: 604.5059  stopTime: 605.2866   stopDistance:  41.1814
For obstacle#15 --- Distance when Visible:49.89941  Sight time: 625.1782  stopTime: 625.9003   stopDistance:  41.85474
For obstacle#16 --- Distance when Visible:49.93921  Sight time: 645.2643  stopTime: 645.9602   stopDistance:  42.21265
For obstacle#17 --- Distance when Visible:49.81079  Sight time: 666.2846  stopTime: 668.59   stopDistance:  23.8606

For obstacle#0 --- Distance when Visible:49.79883  Sight time: 125.4202  stopTime: 208.1868   stopDistance:  -886.4655
For obstacle#1 --- Distance when Visible:49.90439  Sight time: 145.2981  stopTime: 208.1868   stopDistance:  -661.4655
For obstacle#2 --- Distance when Visible:49.87823  Sight time: 165.1874  stopTime: 208.1868   stopDistance:  -436.4655
For obstacle#3 --- Distance when Visible:49.97278  Sight time: 185.0668  stopTime: 208.1868   stopDistance:  -211.4655
For obstacle#4 --- Distance when Visible:49.7981  Sight time: 204.9697  stopTime: 208.1868   stopDistance:  13.53455
For obstacle#5 --- Distance when Visible:49.85071  Sight time: 228.4604  stopTime: 251.3777   stopDistance:  -209.2856
For obstacle#6 --- Distance when Visible:49.95703  Sight time: 248.3404  stopTime: 251.3777   stopDistance:  15.71436
For obstacle#7 --- Distance when Visible:49.96094  Sight time: 270.3328  stopTime: 293.5951   stopDistance:  -213.1162
For obstacle#8 --- Distance when Visible:49.84851  Sight time: 290.2302  stopTime: 293.5951   stopDistance:  11.88379
For obstacle#9 --- Distance when Visible:49.80786  Sight time: 310.9789  stopTime: 314.209   stopDistance:  13.3645
For obstacle#10 --- Distance when Visible:49.96631  Sight time: 333.1019  stopTime: 341.2105   stopDistance:  -41.66211
For obstacle#11 --- Distance when Visible:49.85278  Sight time: 353.0229  stopTime: 376.1105   stopDistance:  -211.2251
For obstacle#12 --- Distance when Visible:49.95972  Sight time: 372.9006  stopTime: 376.1105   stopDistance:  13.7749
For obstacle#13 --- Distance when Visible:49.92969  Sight time: 394.9035  stopTime: 398.3242   stopDistance:  11.3186
For obstacle#14 --- Distance when Visible:49.91602  Sight time: 415.925  stopTime: 418.959   stopDistance:  15.67358
For obstacle#15 --- Distance when Visible:49.80322  Sight time: 436.6049  stopTime: 439.9169   stopDistance:  12.41699
For obstacle#16 --- Distance when Visible:49.85083  Sight time: 457.5392  stopTime: 460.7901   stopDistance:  13.16919
For obstacle#17 --- Distance when Visible:49.99707  Sight time: 479.7132  stopTime: 489.4996   stopDistance:  -60.65088
```

Figure 52b Experimental response output from VR simulation

Analysis- As we can see from the data under 4500K and 6000K subjects identified objects better than 3000K. Here 0 -5 is under 3000K, 6- 11 is under 4500K and 12-17 is under 6000K. The negative value in the stop distance indicates the number of missed objects and the response time is the difference between stop time and sight time.

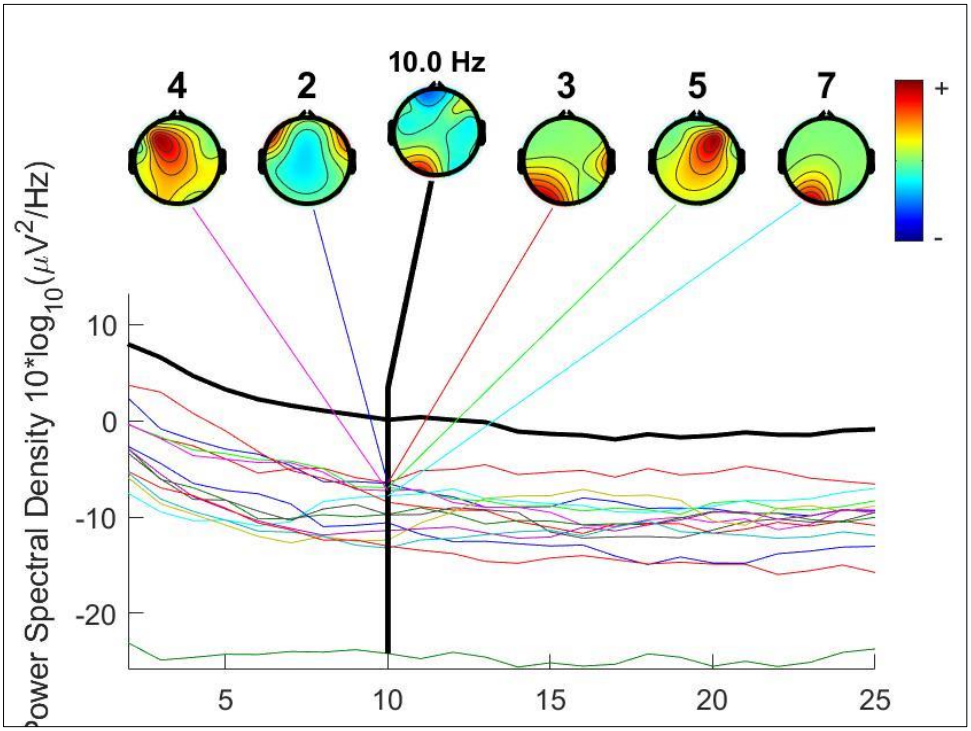

Figure 53 Power Spectral Density vs Frequency

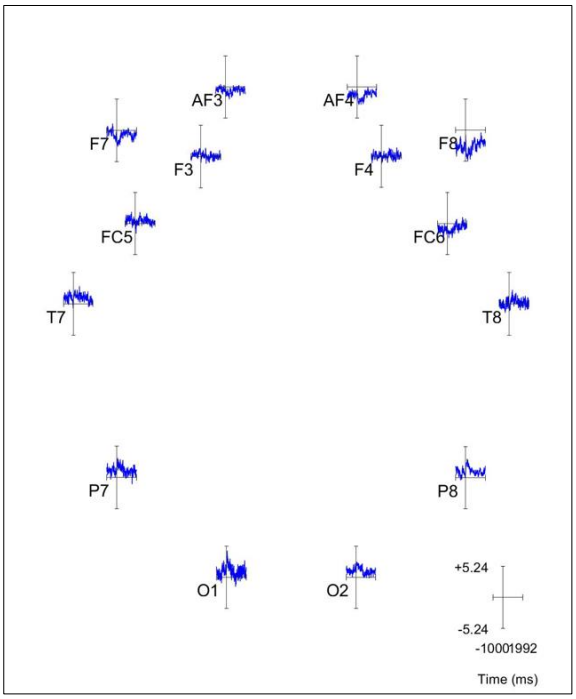

Figure 54 Event related potential plot of VR streetlight simulation

Table 3 GSR average values of eight subjects

GSR average values
496.3
448.25
276.05
269.47
348.15
366.63
402.9
339.23

CHAPTER 9

9.1 Conclusion:

In this thesis two main kinds of study regarding human centric lighting in which the effect of CCT in neurocognitive and behavioural performance are observed. lighting research can be also done in a virtually simulated environment this being validated with the real time experiment is also observed here. First and foremost, effect of CCT in Landolt's based experiment where under four different kinds of CCT 3000K, 4000K, 5000K and 6000K in real time and virtually studied where reaction time, neurocognitive data which EEG data and electrodermal data which is GSR data are studied. It was found that under higher CCTs i.e, 5000K and 6000K where alpha and beta waves were prominently observed, with notable activity in the frontal and occipital regions of the brain. The average GSR data aligned with the EEG findings, indicating improved performance under 5000K and 6000K lighting conditions. Additionally, it was noted that alertness progressively heightened with an increase in correlated colour temperature (CCT). Both real-time and virtual simulations yielded consistent results.

In the second part of the research, a virtual human-centric street lighting simulation was conducted under three different CCTs: 3000K, 4500K, and 6000K. This study focused on testing peripheral vision by having participants identify cuboidal objects on the road. The results, based on EEG, GSR, and response data, indicated that under 4500K and 6000K, especially at 6000K, the maximum number of objects was successfully identified. This suggests that higher CCTs enhance peripheral vision and object detection in driving scenarios.

Thus, it can be concluded that human-centric lighting research can effectively be conducted in a virtually simulated environment. While real-time projects demand significant resources, VR offers a cost-effective and scalable tool for preliminary studies, allowing researchers to refine and expand their work before committing to large-scale experimentation.

9.1 Future scope:

In future research, additional biological parameters such as pulse oximeter and eye tracking could be incorporated alongside EEG, GSR, and VR to gain deeper insights into human-centric lighting. These tools would allow for a more comprehensive understanding of how lighting affects physiological responses and cognitive functions.

The next step for the street lighting experiments would be to conduct real-time experimental validations of the VR simulations. This would help confirm the findings and ensure that the virtual results accurately reflect real-world scenarios.

Data analysis can be further refined by employing more sophisticated methods, such as the Welch's method and k-nearest neighbours (KNN) algorithm, to enhance the accuracy and reliability of the results.

Since lighting plays a crucial role in our daily lives, the applications of virtual reality extend beyond research and into areas like training, education, space exploration, and medical research, where it can be a valuable tool for innovation and discovery.

REFERENCES

Automotive Lighting and Human Vision Burkard Wördenweber Jörg Wallaschek Peter Boyce Donald Hoffman

Federica Nenna, Valeria Orso, Davide Zanardi, Luciano Gamberini. The virtualization of human–robot interactions: a user-centric workload assessment Virtual Reality (2023) 27:553–571

Frey, N. W. (1932). A comparative study of the colour zones and the form zones in peripheral vision. Doctoral dissertation, Massachusetts State College.

Guido Bozzelli, Antonio Raia, Stefano Ricciardi, Maurizio De Nino, Nicola Barile, Marco Perrella, Marco Tramontano, Alfonsina Pagano, Augusto Palombini An Integrated VR/MR Framework for User-Centric Interactive Experience of Cultural Heritage: The ArkaeVision project. Digital Applications in Archaeology and Cultural Heritage (2019) Vol 24 e00124

Human Factors in Lighting_Peter Boyce

IS 3646 (Part 1): 1992

IS:1944 (Parts I amd EI)-1970

Jason Lawrence, Danb Goldman, Supreeth Achar, Gregory Major Blascovich, Joseph G. Desloge, Tommy Fortes, Eric M. Gomez, Sascha Häberling, Hugues Hoppe, Andy Huibers, Claude Knaus, Brian Kuschak, Ricardo Martin Brualla, Harrisnover, Andrew Ian Russell, Steven M. Seitz, And Kevin Tong Project starline: a high-fidelity telepresence system (2021) 1–16

Johnson, J. (2010). Designing with the mind in mind: simple guide to understanding user interface design rules. Elsevier.

Josh Andres, m.c. Schraefel, Nathan Semertzidis, Brahmi Dwivedi, Yutika C Kulwe, Juerg von Kaenel, Florian ‘Floyd’ Mueller CHI 2020, April 25–30, 2020, Honolulu, HI, USA

KW Houser, PR Boyce, JM Zeitzer and M Herf Human-centric lighting: Myth, magic or metaphor? Lighting Res. Technol. 2020; 1–22

Nannan Xi, Juho Hamari Shopping in virtual reality: A literature review and future agenda Journal of Business Research 134 (2021) 37–58

NLC (National Lighting Code) 2010

Rosenholtz, R. (2016). Capabilities and limitations of peripheral vision. Annual Review of Vision Science, 2, 437-457.

S Fotios PhD and C Cheal PhD, Obstacle detection: A pilot study investigating the effects of lamp type, illuminance and age, Lighting Res. Technol. 2009; 41: 321–342

Snježana IVANČIĆ VALENKO, Vladimir CVILJUŠAC, Sanja ZLATIĆ, Damir MODRIĆ, The Impact of Physical Parameters on the Perception of the Moving Elements in Peripheral Part of the Screen, Article · May 2020, Researchgate

Solso, R. L. (1996). Cognition and the visual arts. The MIT press. Cambridge, London

Suddhasatwa Chakraborty, Debtanu Ray, Ishan Palit An EEG based comparative study on driver's performance under the influence of metal halide and high pressure sodium lighting, Optik - International Journal for Light and Electron Optics 245 (2021) Jadavpur University, Illumination Engineering Laboratory, Department of Electrical Engineering, India.

The IESNA Lighting Handbook 10th edition David L. DiLaura, Kevin W. Houser, Richard G. Mistrick, Gary R. Steffy

van Bommel, W. (2015). Purpose and Benefits of Road Lighting. In: Road Lighting. Springer, Cham.

W Adrian Lighting Research and Technology Volume: 21Issue Number: 4Publisher: Sage Publications Limited

Xiaojun Li, Jiaxin Ling, Yi Shen, Tong Lu, Shouzhong Feng, Hehua Zhu The impact of CCT on driving safety in the normal and accident situation: A VR-based experimental study Advanced Engineering Informatics 50 (2021) 101379

ANNEXURES

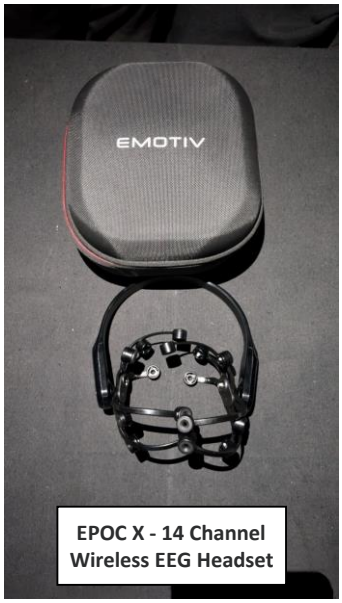

EPOC X - 14 Channel Wireless EEG Headset

The EEG headset features 14 channels, including AF3, F7, F3, FC5, T7, P7, O1, O2, P8, T8, FC6, F4, F8, and AF4, with CMS/DRL references at P3/P4 and alternative references at the left/right mastoid process. The sensors use saline-soaked felt pads. Connectivity is wireless via Bluetooth® Low Energy, with support for Bluetooth® 5.0 in upcoming updates, and a proprietary USB receiver operating in the 2.4GHz band. USB is also available for changing headset settings and using an extender. The EEG signals are sampled sequentially through a single ADC, with a sampling rate of 2048, down sampled to 128 or 256 SPS. The resolution is 0.51µV in 14-bit mode and 0.1275µV in 16-bit mode. The bandwidth ranges from 0.16 to 43Hz, with digital notch filters at 50Hz and 60Hz, and a built-in digital 5th order Sync filter. The dynamic range is 8400 µV(pp), and the signals are AC-coupled. The motion sensor includes the ICM-20948 IMU, providing normalized, 4D quaternions with 16-bit resolution. Available detections include up to four pre-trained mental commands, performance metrics like excitement, engagement, relaxation, interest, stress, and focus, as well as facial expressions such as blinking, winking, surprise, frowning, smiling, clenching, laughing, and smirking. The headset is powered by a 595mAh internal lithium polymer battery, offering up to 12 hours of battery life with the USB receiver and up to 6 hours with Bluetooth Low Energy. The device weighs 170g and measures 9 x 15 x 15 cm, with limited beta support for Ubuntu and Raspberry Pi, subject to OS changes.

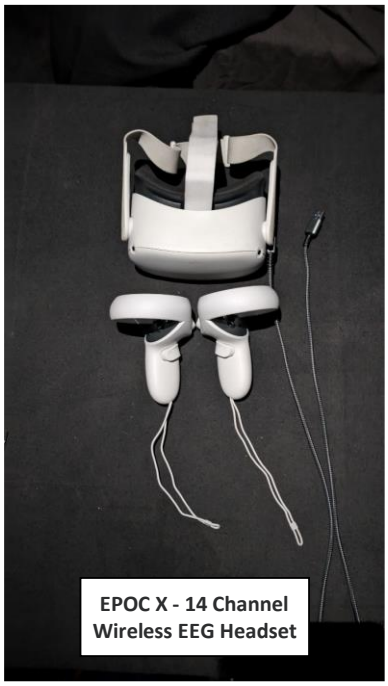

EPOC X - 14 Channel Wireless EEG Headset

The product details include 4 AA batteries required, which are included with the item. It has dimensions of 26 x 18.7 x 12.6 cm and weighs 830.07 g. The release date is 25 August 2021, and the ASIN is B099VMT8VZ. The item model number is 899-00182-02, manufactured by Meta Quest under the brand META. The net quantity is 1 count, and the included components are a VR headset, 2 controllers, and a charger. The generic name for this product is a Virtual Reality Headset. Storage is 128 GB.

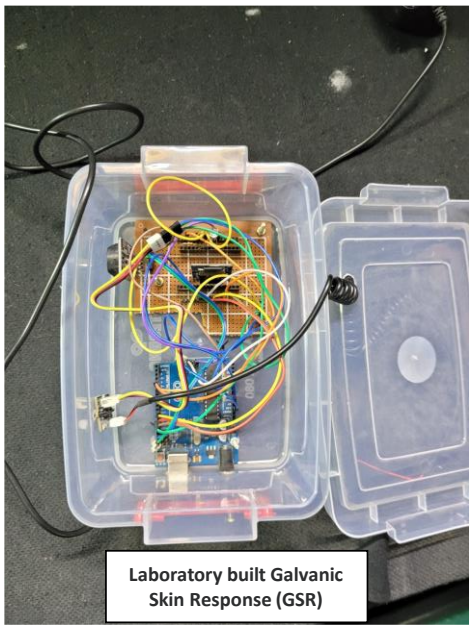

Laboratory built Galvanic Skin Response (GSR)

Specification

Parameter	Value/Range
Operating voltage	3.3V/5V
Sensitivity	Adjustable via a potentiometer
Input Signal	Resistance, NOT Conductivity
Output Signal	Voltage, analog reading
Finger contact material	Nickel

Circuit diagram

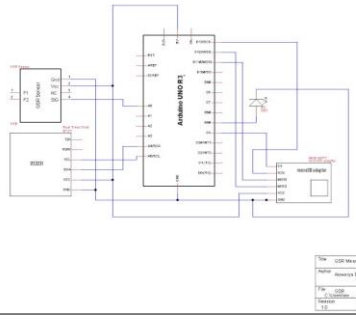

CRI Illuminance Meter CL-70F

Model	CL-70F CRI Illuminance Meter
Illuminance meter class	Conforms to requirements for Class A of JIS C1609-1：2006 "Illuminance meters Part1:General measuring instruments; Conforms to DIN 5032 Part 7 Class C
Sensor	CMOS linear image sensor
Spectral wavelength range	380 to 780 nm
Output wavelength pitch	1 nm
Measuring range	Constant light: 1 to 200,000 lx; 1,563 to 100,000 K (Chromaticity display requires 5 lx or more) Flash light: 20 to 20,500 lx • s; 2,500 to 100,000 K
Accuracy *1, 2 (Standard illuminants A)	Ev (Illuminance) : +-5%+-1 digit of displayed value xy: 0.003 (at 800 lx)
Repeatability (2 σ) (Standard illuminant A)	Ev: 30 to 200,000 lx: 1%+1digit; 1 to 30 lx: 5%+1digit (*3) xy: 500 to 200,000 lx: 0.001 (*4) xy: 100 to 500 lx: 0.002 (*4) xy: 30 to 100 lx: 0.004 (*4) xy: 5 to 30 lx: 0.008 (*4)
Visible-region relative spectral response characteristics (f1')	Within 9%
Cosine response (f2)	Within 6%
Temperature drift (fT)	Ev: +-5% of displayed value; xy: +-0.006
Humidity drift (fH)	Ev: +-3% of displayed value; xy: +-0.006
Power	2 AA-size batteries (Alkaline batteries or manganese dry cells); USB bus power
Response Time	Constant light (Maximum): 15 sec Constant light (Minimum): 0.5 sec Flash light: 1 ~ 1/500 sec (in 1-step intervals) (*5)
Color indication modes	Correlated color temperature Tcp, Difference from blackbody Δ uv, XYZ, xy, u'v', Dominant wavelength λ d, Excitation purity Pe, Spectral irradiance, Ev, CRI (Ra, Ri), Peak wavelength λ p, exposure value
Other functions	Data memory: 999 data; Preset function; Auto power off function
Display languages	English, Japanese, Chinese (Simplified)
Interface	USB 2.0 Mini B
Operation temperature/humidity range	-10 to 40°C, relative humidity of 85% or less (at 35°C) with no condensation
Storage temperature/humidity rangen	-10 to 45° C, relative humidity 85% or less (at 35° C) with no condensation
Dimensions (W x H x D)	73 x 183 x 27 mm (Not including projecting buttons) D (max): 40mm
Weight	230 g
*1 Measurement mode: Constant light (range L), Exposure time: AUTO	
*2 Linear for Ev	
*3 10 times measurement (2σ) /Ave	
*4 10 times measurement (2σ)	
*5 Shutter speed	

FLUKE 416D Distance meter

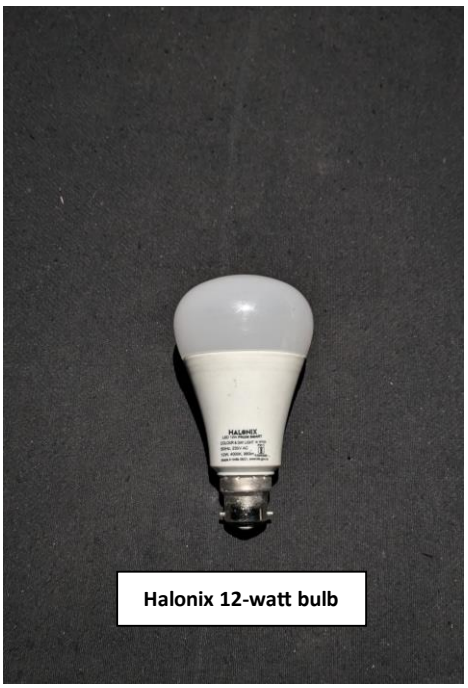

Halonix 12-watt bulb

Halonix 12-watt bulb:
Base: B22, Color temperature: 6500K, with high lumens 1150Lm
Ideal for reading, working
5 star rating L D Bulb
Light distribution is greater than 300 degree
Provide high surge protection of 3 K (Fluctuation Proof), wide operating voltage (90 300 , 50 z)